Drug Design, Development and Therapy

Dovepress
Taylor & Francis Group

Open Access Full Text Article

ORIGINAL RESEARCH

ShenQi ShenKang Granule Alleviates Chronic Kidney Disease by Inhibiting the PI3K/AKT/mTOR Pathway and Restoring Autophagy Flux and Mitochondrial Integrity

Chenhui Xia[1–3,*], Jiale Zhang[1–3,*], Huixi Chen[1–3], Shaofeng Zhou[1–3], Weimin Jiang[1–3], Huijuan Zheng[1–3], Zaoqiang Lin[4], Qinxiang Tan[4], Weiwei Sun[1–3]

[1]Department of Nephrology, Dongzhimen Hospital Affiliated to Beijing University of Chinese Medicine, Beijing, People's Republic of China; [2]Department of Renal Research, Dongzhimen Hospital Affiliated to Beijing University of Chinese Medicine, Beijing, People's Republic of China; [3]Key Laboratory of Chinese Internal Medicine of Ministry of Education and Beijing, Dongzhimen Hospital Affiliated to Beijing University of Chinese Medicine, Beijing, People's Republic of China; [4]Department of Nephrology, Shenzhen Hospital Affiliated to Beijing University of Chinese Medicine, Shenzhen, Guangdong, People's Republic of China

*These authors contributed equally to this work

Correspondence: Weiwei Sun, Department of Nephrology, Dongzhimen Hospital Affiliated to Beijing University of Chinese Medicine, Beijing, People's Republic of China, Email sunweitcm@163.com; Qinxiang Tan, Department of Nephrology, Shenzhen Hospital Affiliated to Beijing University of Chinese Medicine, Shenzhen, Guangdong, People's Republic of China, Email 20220941170@bucm.edu.cn

Purpose: This study investigates the effect of Shenqi Shenkang granule (SQSKG) on chronic kidney disease (CKD), focusing on regulating the PI3K/AKT/mTOR pathway, autophagy, and mitochondrial homeostasis.

Methods: The compounds and targets of SQSKG on CKD were identified by network pharmacology and validated by molecular docking. LC-MS/MS was used to verify the compounds screened by network pharmacology. In vitro experiments based on HK-2 cells were used to assess its impact on cell migration, viability, oxidative stress, and key proteins of the PI3K/AKT/mTOR pathway, autophagy, and fibrosis. Mitochondrial function and autophagic flux were evaluated via JC-1, Mito-Tracker, and Ad-mCherry-GFP-LC3B assays. In vivo, an adenine-induced CKD rat model was used to analyze renal function, fibrosis, and autophagy through serum/urine tests, histology, and immunofluorescence.

Results: Network pharmacology identified 49 compounds and 149 targets associated with SQSKG's therapeutic effects on CKD, highlighting critical targets such as AKT1, MAPK1, EGFR, HSP90AA, and IGF1R. The primary mechanism involves the PI3K/AKT pathway. In vitro experiments demonstrated that SQSKG significantly enhanced cell migration, colony formation, viability in AGEs-treated HK-2 cells, and exhibited robust antioxidant properties by increasing SOD levels and reducing MDA and ROS production. SQSKG effectively inhibited the phosphorylation of PI3K, AKT, and mTOR, and reduced TGF-β fluorescence intensity in kidney tissue. Autophagic flux analysis showed that SQSKG increased autophagic activity and reduced p62 accumulation. Additionally, JC-1 and Mito-Tracker Green assays demonstrated that SQSKG improved mitochondrial membrane potential and morphology. In vivo, SQSKG significantly improved renal function and alleviated renal fibrosis in a dose-dependent manner, reversing fibrosis marker overexpression (Col-I, α-SMA, TGF-β) and activating autophagy.

Conclusion: Our findings provide novel insights into the therapeutic potential of SQSKG in CKD management, highlighting its ability to modulate PI3K/AKT/mTOR pathway, activating autophagy flux, and restoring mitochondrial integrity, thereby offering a promising complementary or alternative treatment option for patients with CKD.

Keywords: Shenqi Shenkang Granule, chronic kidney disease, network pharmacology, renal fibrosis, PI3K/AKT/mTOR pathway, autophagy

Received: 30 December 2024
Accepted: 12 May 2025
Published: 15 May 2025

Graphical Abstract

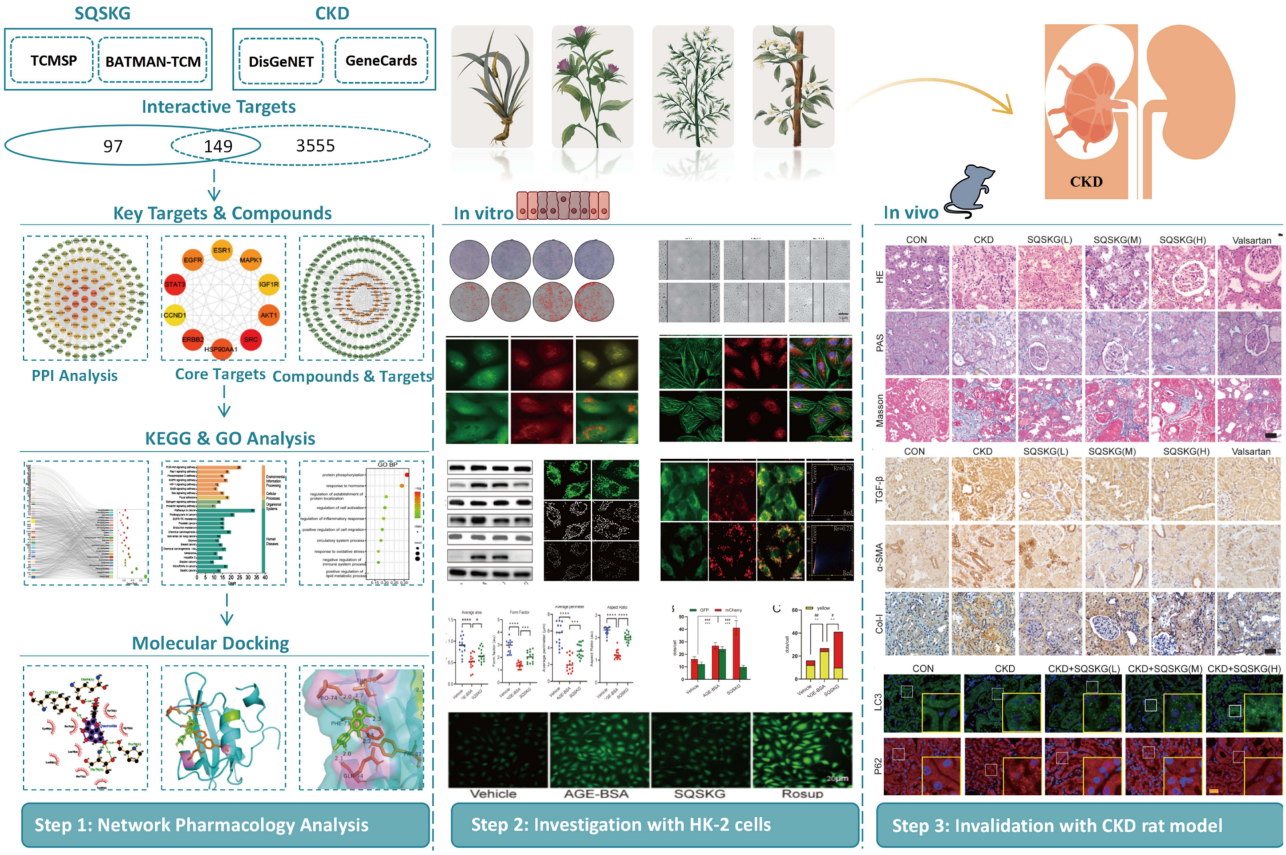

Introduction

Chronic kidney disease (CKD) is characterized by a gradual decline in the glomerular filtration rate, ultimately culminating in end-stage renal disease (ESRD). In recent years, there has been a significant increase in the incidence and hospitalization rate of patients with ESRD.[1] The progression of CKD is intricately linked to the severity of renal fibrosis induced by diverse risk factors such as inflammation, angiotensin (ANG), advanced glycation end products (AGEs), and parathyroid hormone (PTH).[2,3] Persistent and excessive renal fibrosis can potentially disrupt the normal kidney architecture, leading to the loss of functional nephrons and resulting in abnormal blood filtration, fluid-electrolyte balance regulation, and waste excretion.[4] Current CKD treatment primarily focuses on blood pressure and glucose control, dietary and lifestyle modifications, addressing complications, or resorting to dialysis and transplantation.[5] However, strategies for directly addressing or mitigating damage to renal cells caused by various stimuli still necessitate further research. Therefore, understanding the underlying mechanisms of fibrosis and developing effective therapeutic interventions to regulate it remains crucial.

In traditional Chinese medicine (TCM), CKD is classified as "deficiency fatigue" or "edema". This reflects the TCM view that CKD is associated with a deficiency in kidney function or vital energy and an excess of pathogenic water. It is diagnosed in TCM by identifying specific patterns such as qi deficiency, blood stasis, and dampness accumulation.[6] "Shenqi Dihuang Tang", a formula from the Chinese medical text "Zabing Xizhu", is commonly utilized as a fundamental prescription for treating CKD, aiming to tonify qi, nourish yin, and strengthen the kidneys and spleen.[7] However, due to its insufficient power to promote blood circulation and remove stasis, it is often modified by modern Chinese medicine practitioners to treat CKD.[8] Based on clinical practice, we optimized it into "Shenqi Shenkang Granule

(SQSKG)" by reinforcing the capacity of tonifying qi (*Yiqi*) and invigorating blood circulation (*Huoxue*). The prescription comprises *Astragalus mongholicus* Bunge (Huang qi), *Codonopsis pilosula* Nannf. (Dang shen), *Salvia miltiorrhiza* Bge. (Dan shen), *Atractylodes macrocephala* Koidz. (Bai zhu), *Poria cocos* (Schw). Wolf (Fu ling), *Angelica sinensis* (Oliv). Diels (Dang gui), *Paeonia lactiflora* Pall. (Chi shao), *Paeonia suffruticosa* Andrews (Mu dan pi), *Rehmannia glutinosa* (Gaertn). DC. (Shu di huang), *Eclipta prostrata* (L). L. (Mo han lian), *Ligusticum striatum* DC. (Chuan xiong), and *Coix lacryma-jobi* L. (Yi yi ren). Detailed information is listed in Table 1. Our previous clinical study of 86 CKD patients demonstrated SQSKG's potential benefits. All patients received standard CKD treatment, with the control group given a placebo and the observation group given SQSKG. SQSKG significantly improved renal function by reducing serum creatinine (SCR), blood urea nitrogen (BUN), and creatinine clearance rate (Ccr) levels and downregulating TGF-β and miR-21. These findings suggest it may alleviate renal fibrosis and slow CKD progression through distinct molecular pathways.[9] The significant effectiveness of SQSKG has led to its approval for TCM record-keeping management (No. Z20220006000) by the local Medical Products Administration (https://mpa.gd.gov.cn/wycxh5/yjj-pc/#/data). Recent clinical studies further support the potential of herbal medicine in CKD treatment. A meta-analysis of 34 studies (2786 patients) demonstrated that rhubarb-based therapy significantly reduced SCR, BUN, and uric acid (UA) while improving Ccr and overall symptom relief.[10] Another meta-analysis of 32 trials (2264 participants) showed that Salvianolate and Tanshinone, as complementary therapies, enhanced renal function and delayed CKD progression without significant adverse effects.[11] These findings highlight the therapeutic potential of herbal medicine in CKD. The beneficial effect of herbal medicine might be associated with its capacity to alleviate inflammation, fibrosis, and apoptosis.[12,13] Therefore, the precise molecular mechanism behind the effectiveness of SQSKG prescription requires a deeper understanding.

Research on kidney disease is concentrated on halting the progression of renal fibrosis, a complex pathogenic process intertwined with the interaction of diverse damaging stimuli, oxidative stress, mitochondrial dysfunction, and dysregulation of autophagy.[14,15] Meanwhile, herbal medicines comprise numerous bioactive compounds that target multiple signaling pathways, posing a challenge in examining their effects and potential mechanisms on diseases. Fortunately, the prevalence of network pharmacology has assisted researchers in unraveling the intricate mechanisms of herbal medicines.[16] Several herbs in SQSKG have been estimated by network pharmacological analysis. One study revealed that Angelicae Sinensis Radix and Chuanxiong Rhizoma possess 13 bioactive compounds, with targets and pathways primarily linked to anti-fibrosis and anti-inflammatory effects.[17] Another pharmacological study indicated that Radix Salviae targets are mainly associated with angiogenesis, protein metabolism, inflammatory response, apoptosis, and cell proliferation.[18] Yet, a solitary herbal medicine cannot achieve an effective outcome as the entire prescription. Therefore, this study investigates whether SQSKG can manifest a more comprehensive and distinctive anti-fibrosis effect in treating CKD.

Table 1 The Information on Herbal Medicines in SQSKG

Botanical Plant Names	Family	Part Used	Voucher Number	Dose(g)
Astragalus mongholicus Bunge	Leguminosae	Dried root	Shandong7170104	30
Codonopsis pilosula Nannf.	Campanulaceae	Dried root	Gansu7170103	15
Salvia miltiorrhiza Bge.	Lamiaceae	Dried root	Hebei71205	10
Atractylodes macrocephala Koidz.	Asteraceae	Dried root	Zhejiang7170106	10
Poria cocos (Schw.) Wolf	Polyporaceae	Dried Sclerotium	Anhui7010604	20
Angelica sinensis (Oliv.) Diels	Umbelliferae	Dried root	Gansu7170301	10
Paeonia lactiflora Pall.	Ranunculaceae	Dried root	Neimenggu7020305	10
Paeonia suffruticosa Andrews	Ranunculaceae	Dried root bark	Anhui7020304	10
Rehmannia glutinosa (Gaertn.) DC.	Scrophulariaceae	Dried root tuber	Henan7170304	15
Eclipta prostrata (L.) L.	Compositae	Dried ground body	Hebei7170417	10
Ligusticum striatum DC.	Umbelliferae	Dried root	Sichuan71201	10
Coix lacryma-jobi L.	Gramineae	Dried mature seed	Guizhou70603	20

Note: The botanical plant names of herbs have been checked by The Plant List (https://www.theplantlist.org/).

Network pharmacology provides a comprehensive insight into the complex interactions between bioactive compounds and multiple targets within biological systems. However, its accuracy depends on computational models, which may not always accurately reflect real-world biological complexities.[19] This study adopted a comprehensive approach to enhance reliability, combining literature research and database searches to identify compounds in SQSKG. Strict criteria were employed for target prediction, and molecular docking was utilized to assess affinity in compound-target interactions. Quality control of pharmacological components achieved by LC-MS. Crucially, the study incorporated in vivo and in vitro experiments to validate results and delve into the deeper bio mechanisms of SQSKG in treating CKD.

Materials and Methods

Network Pharmacology Analysis

Bioactive compounds from each herb in SQSKG were screened from TCMSP (https://old.tcmsp-e.com/tcmsp.php) and BATMAN-TCM (http://bionet.ncpsb.org.cn/batman-tcm/index.php) based on oral bioavailability (OB) ≥ 30% and drug-likeness (DL) ≥ 0.18. Compounds that do not meet the screening criteria but exhibit significant bioactivity according to the literature were included. The potential targets of the compounds were obtained from the SwissTarget Prediction database (https://www.swisstargetprediction.ch/index.php) with a probability ≥ 0.5. Target names were unitized by the UniProt database (https://www.uniprot.org/). CKD disease targets were obtained from DisGeNET (https://www.disgenet.org/) and GeneCards (https://www.genecards.org/) and combined to remove duplicates. Common targets of SQSKG and CKD were obtained through Venn plots. The drug-compound-target network was constructed using Cytoscape 3.9.1 software. Subsequently, the protein-protein interaction analysis (PPI) of the drug-disease intersection targets was conducted using the STRING database (https://cn.string-db.org/) with "Homo sapiens" and a high confidence score (0.7). The networks were analyzed through "Network Analyzer" in Cytoscape 3.9.1. The Gene Ontology (GO) and Kyoto Encyclopedia of Genes and Genomes (KEGG) pathway enrichment analyses of the intersection targets were performed using Metascape (https://metascape.org/) and were visualized using the Bioinformatics platform (http://www.bioinformatics.com.cn/).

Molecular Docking Validation

This study assessed the adaptability of two different molecular structures through the standard molecular docking method. AutoDock 4.2.6 (http://autodock.scripps.edu/) analyzed binding affinities and interaction modes between core compounds and targets. Compound molecular structures were obtained from PubChem (https://pubchem.ncbi.nlm.nih.gov/), while 3D structures of protein targets were downloaded from the PDB database (http://www.rcsb.org/). In preparation for docking analysis, all protein and molecular files were converted into PDBQT format, excluding water molecules and adding polar hydrogen atoms. The grid box was centered to cover each protein's domain and allow free molecular movement. AutoDock 4.2.6 was employed for molecular docking studies, and PyMOL software was used for result visualization. Additionally, LigPlot 2.2 was utilized to create 2D ligand-protein interaction diagrams.

Chemicals and Reagents

SCR and BUN detection kits were bought from Nanjing Jiancheng Bioengineering Institute (C011-2, C013-1-1, Nanjing, China). The urine albumin detection kit was bought from Abcam (ab108789, Shang, China). AGE-BSA was bought from Cayman (22968, Beijing, China). Superoxide dismutase (SOD) assay kit (S0101S), Malondialdehyde (MDA) assay kit (S0131S), Ad-mCherry-GFP-LC3B kit (C3011), Mitochondrial membrane potential assay kit (C2006), Mito-tracker green (C1048), and Reactive oxygen species assay kit (S0033S) were bought from Beyotime (Shanghai, China). Hoechst 33258 staining solution was bought from Solarbio (C0021, Beijing, China). A mounting medium with DAPI was bought from Abcam (ab104139, Shanghai, China). Antibodies are as follows: PI3K (4257), p-PI3K (17366), AKT (4685), p-AKT (13038), mTOR (2983), and p-mTOR (5536) were bought from Cell Signal Technology (Shanghai, China); Transforming growth factor-β (TGF-β) (21,898-1-AP), α-smooth muscle actin (α-SMA) (14,395-1-AP), collagen-I (Col-I) (14,695-1-AP), Bcl-2-associated X protein (Bax) (50,599-2-Ig), Cysteine-aspartic acid protease-3 (caspase-3) (19,677-

1-AP), and β-actin (66009-1-Ig) were bought from Proteintech (Wuhan, China); microtubule-associated protein I light chain 3 (LC3) (ab192890), Beclin-1 (ab207612), and p62 (ab109012) were bought from Abcam (Shanghai, China).

Preparation and Composition Analysis of SQSKG

SQSKG was obtained from Dongzhimen Hospital of Beijing University of Chinese Medicine; detailed information is displayed in Table 1. Their qualities have been verified through the hospital pharmacies. After soaking in distilled water for one hour, the herbs were twice decocted for one hour (1:10, w/v). The w/w yield of SQSKG was 15.6%. The filtrates were concentrated at 1 g/mL. The dosage of SQSKG used in rats was converted from the clinical dosage according to literatures.[20,21] Briefly, the high dosage of SQSKG = 6.3×131 g/70kg. The equivalent dose ratio for humans and rats was 6.3. The clinical dosage was 131 g/day for a 70 kg adult. The middle and low doses of SQSKG were set at half and a quarter of the high dose (SQSKG-H), respectively. For in vitro experiments, the extraction solution was processed using the lyophilization method. This method employed low heat to eliminate unnecessary solvents. The solution was frozen, then a vacuum was applied to dry the product. This condition contributed to product stabilization and minimized the impact of oxidation, thus preserving product quality. The lyophilized powder was stored in airtight vials and dissolved in DMEM for the in vitro experiments.

The composition analysis of SQSKG was performed using LC-MS/MS (Vanquish, Thermo Fisher Scientific). The details of the MS analysis are provided in the Supplementary Method 1.

Animals

Animal studies adhered to the ARRIVE guidelines, and the experimental protocol received approval from the Experimental Animal Ethics Committee of the Beijing University of Chinese Medicine (Permit Number: BUCM-2023090709-3229). Adult male Sprague Dawley (SD) rats weighing 230–240 g were purchased from Beijing Vital River Laboratory Animal Technology Co., Ltd (Beijing, China). All animals were housed in controlled laboratory conditions (22–25°C, 12 h light/dark cycles, 50–60% humidity) and provided free access to approved ordinary chow and water for a minimum of seven days.

CKD Model and Interventions

Animals were fed a 0.25% adenine diet for 16 weeks, a duration shown to induce progressive kidney damage, mimicking CKD's slow development in humans (≈8 years).[22,23] This model leads to increased SCR, BUN, potassium, and lactate dehydrogenase (LDH) activity. Structurally, it causes tubular atrophy, proximal tubular brush border erosion, epithelial flattening, focal hypertrophy, and glomerulosclerosis, closely resembling human CKD pathology and making it suitable for studying disease progression and treatments.[24] Rats were divided into 6 groups: normal control group (CON, n = 10), model group (CKD, n = 10), 2.95 g/kg SQSKG treatment group (SQSKG-L, n = 10), 5.89 g/kg SQSKG treatment group (SQSKG-M, n = 10), 11.79 g/kg SQSKG treatment group (SQSKG-H) and 0.72 mg/100g Valsartan treatment group (Valsartan, n = 10). Both SQSKG and Valsartan were dissolved in distilled water. The SQSKG treatment group and the Valsartan treatment group were given oral doses once a day for the last 8 weeks. The normal control group and CKD group were treated with the equivalent volume of saline. At the end of the experiments, animals were anesthetized with pentobarbital.

Biochemical Analysis

Upon completion of the experiment, blood and urine samples were collected, centrifuged at 4°C for 15 minutes at a speed of 3500 rpm, and retained for subsequent analysis. The levels of biochemical indexes (SCR, BUN, urinary protein) were assessed using detection kits following the manufacturer's instructions.

Histology Examination

After 4% paraformaldehyde fixation, the kidney tissue was dried, embedded in paraffin, sliced, dewaxed, and hydrated. Pathological changes were observed through Hematoxylin-eosin (H&E) and periodic acid-Schiff (PAS) staining.

Masson's trichrome staining was applied to evaluate fibrosis in each section. Images were captured using a Zeiss optical microscope. Pathophysiological kidney injuries were assessed using previously established methods.[12]

Immunohistochemistry

The kidney tissues were processed as above. Next, its antigen was removed, blocked, and incubated at 4°C overnight with a primary antibody. After being washed three times in PBS, sections were exposed to HRP-conjugated secondary antibodies at 37°C for one hour. The reaction was developed using a DAB solution for 5 minutes at room temperature. Finally, the tissue sections underwent dehydration, clearing, and mounting. Images were captured using a Zeiss optical microscope and analyzed using Image-Pro Plus 6.0 software (Media Cybernetics, USA).

Immunofluorescence

The paraffin-embedded kidney tissues were processed as described above. Triton X-100 (0.1%) was introduced to enhance cell membrane permeability. Following a 1-hour incubation with blocking serum at room temperature, the sections were stained with primary antibodies at 4°C overnight. Subsequently, goat anti-rabbit/mouse IgG (H+L) secondary antibodies were applied for 2 hours. The slides were then mounted with an antifade mounting medium containing DAPI. In in vitro experiments, cells were washed with PBS buffer, fixed in 4% ice-cold paraformaldehyde, permeabilized with 0.1% Triton X-100, and blocked with 5% bovine serum albumin (BSA). The slides were incubated with primary antibodies targeting TGF-β and p62 at 4°C overnight. Afterward, secondary antibodies labeled with Alexa Fluor 488/594 were applied at room temperature for 2 hours, and the slides were mounted as previously described. Images were captured using an Olympus fluorescence microscope, and fluorescence intensity was analyzed using ImageJ software (National Institutes of Health, USA).

Western Blot

Total proteins were extracted from cells or kidney tissues using RIPA buffer containing protease and phosphatase inhibitors. The protein concentration was determined using a BCA protein detection kit. Proteins were separated through SDS-PAGE and transferred onto a PVDF membrane. After being blocked with 5% BSA, the membranes were incubated with primary antibodies at 4°C overnight. Following three TBST washes, an HRP-labeled secondary antibody (1:8000) was applied to the membranes for 1 hour at room temperature. Visualization was achieved using an ECL kit. Protein intensities were then measured using Image J software. All experiments were repeated four times.

Cell Culture

Renal Tubular Epithelial Cells HK-2 (ATCC, Manassas, VA) were cultured in a 25 cm^2 flask supplemented with DMEM medium and 10% heat-inactivated FBS, including 100 U mL^{-1} penicillin/streptomycin (P/S). The cells were incubated in a 5% CO_2 atmosphere at 37°C. The medium was refreshed every two days.

Cell Viability

Cell viability was assessed using a CCK-8 kit following the recommended protocol. Briefly, 100 mL of cells (1×10^5 cells/well) in DMEM were cultured in a 96-well plate and incubated overnight. After treatment with specified concentrations (25, 50, 100 μg/mL) of SQSKG (dissolved in DMEM) for a specific period (0, 24, 48 h), the medium was discarded, and the plate was washed with PBS. Subsequently, 100 μL of DMEM was added to each well, followed by 10 μL of CCK-8 solution, and incubated for 0.5–1 hour. Additionally, AGE-BSA, acting as a stimuli factor, was added at a concentration of 100 μg/mL for 12 hours to evaluate the cytoprotective effect of SQSKG. The optical density (OD) value was read with a spectrophotometer (Thermo Fisher, Finland) at 450 nm to determine cell viability in each well.

Colony Formation Assay

The cells were cultured in 9.6 cm^2 plates at 500 cells/well density and incubated overnight. They were then treated with specified concentrations (0, 25, 50, 100 μg/mL) of SQSKG and incubated at 37°C with 5% CO_2 for one week. Once the number of cells in each clone exceeded 50, the culture medium was discarded. Subsequently, the dishes were rinsed twice

with PBS and fixed with 4% paraformaldehyde for 15 minutes. Giemsa staining was applied for 10 minutes, and the excess stain was slowly rinsed away with running water, followed by air drying. The images were analyzed using Image J software.

Wound-Healing Assay

To conduct a cell scratch assay, begin by marking horizontal lines on the bottom of a 6-well plate using a marker. Subsequently, seed cells were placed in a 6-well plate with 2 mL of medium per well and incubated at 37°C with 5% CO_2 for 24 hours. The next day, create scratches along the marked lines using a 200 μL pipette tip, ensuring proper alignment. Wash the cells with PBS and incubate them with a medium containing SQSKG at 100 μg/mL concentration or a corresponding Vehicle. Subsequently, marker lines were removed, images were captured at 0, 12, and 24 hours, and finally, the results were analyzed using Image J software.

Detection of SOD Activity and MDA Levels

The protein of cells was collected for the detection of SOD and MDA in HK-2 cells according to the manufacturer's instructions. A spectrophotometer (Thermo Fisher, Finland) was used to read the absorbance value of SOD at 450 nm and MDA at 532 nm.

Detection of ROS

The cells underwent exposure to AGE-BSA in combination with either SQSKG or Rosup (used as a positive control) for 24 hours. After removing the medium, DCFH-DA was introduced at a concentration of 1:5000 and incubated for 10 minutes at 37°C. Subsequently, the cells were subjected to three washes with serum-free cell culture medium to eliminate any residual DCFH-DA that did not penetrate the cells. Ultimately, the cells were examined under a fluorescence microscope and analyzed using Image J software.

JC-1 Assay

JC-1, a commonly employed fluorescent probe for detecting mitochondrial membrane potential (MMP), was utilized in this study. Cells cultured for 24 hours were treated with AGE-BSA (100 μg/mL) or AGE-BSA plus SQSKG (100 μg/mL) for 24 hours. After medium removal, cells were incubated with the JC-1 fluorescent probe (10 μg/mL) at 37°C with 5% CO_2 for 15 minutes. Following two washes, the cells were observed under a fluorescence microscope. Healthy cells exhibited red fluorescence (590 nm) attributable to JC-1 aggregation, whereas apoptotic or necrotic cells emitted green fluorescence (530 nm). The red-to-green fluorescence ratio was an indicator for assessing cellular health and mitochondrial function.

Detection of Mitochondria

Mitochondrial morphology was visualized using Mito-Tracker. Cells (1×10^5 cells/well) were cultured in a 24-well plate and incubated overnight. Following the treatment with AGE-BSA or AGE-BSA plus SQSKG for 24 hours, RTEC cells were exposed to Mito-Tracker Green (0.5 μM) for 20 minutes. The cells were observed, and images were captured under a fluorescence microscope.

Ad-mCherry-GFP-LC3B Infection Analysis

Autophagic flux was monitored with the adenovirus transfection method. Before transfection, HK-2 cells were seeded at 1×10^5 cells/well in a 24-well plate with 1 mL of complete medium per well to achieve approximately 50% cell confluence on the day of viral infection. After 24 h, the previous medium was discarded, and 1 mL of fresh culture medium was added to each well, followed by Ad-mCherry-GFP-LC3 (40 MOI) for another 24 h. After 24h, the medium was replaced with 1 mL of specific concentrations of AGE-BSA (100 μg/mL) and SQSKG (100 μg/mL). Fluorescence protein expression was observed under a fluorescence microscope after 24 hours of incubation.

Sample Size Analysis

The sample sizes for both in vitro and in vivo experiments were determined using G*Power software (version 3.1.9.7).[25] Effect size was calculated using Cohen's d statistic based on previous studies and preliminary data, using the formula $d = |\mu_1 - \mu_2|/\sigma$, where μ_1 and μ_2 represent the group means, and σ is the pooled standard deviation. Then the effect size was used to conduct a power analysis, with a statistical power ($1-\beta$) of 0.8 and a significance level (α) of 0.05, ensuring an adequate sample size for reliable statistical comparisons.

Statistical Analysis

Statistical analyses were performed using SPSS 29.0, and data are presented as means ± standard deviation (SD), counts, or percentages. All experiments were independently replicated at least three times. Normality was assessed using the Shapiro–Wilk test. Multiple groups meeting the assumption of normality were analyzed using one-way ANOVA, followed by Tukey's HSD test for pairwise comparisons or Dunnett's test when comparing multiple groups to a control. Two-group comparisons were made using an independent sample *t*-test. For multiple comparisons, Bonferroni correction was applied where appropriate to control for Type I errors. Statistical significance was defined as a p-value < 0.05.

Results

Network Pharmacology Analysis

The TCMSP and BATMAN-TCM databases indicate that the 12 herbal medicines contain 1162 bioactive compounds. Upon applying screening criteria (OB $\geq$ 30%, DL $\geq$ 0.18), the number of druggable compounds is reduced to 198. A literature review identified 13 compounds with significant pharmaceutical activity that did not meet the screening criteria but were deemed essential and restored. Subsequently, compounds lacking experimental or predicted targets (possibility > 0.5) were excluded from the analysis, resulting in a total of 64 druggable compounds after eliminating duplicates (Figure 1A and Table S1).

SQSKG's potential targets were 246 after removing duplicates (Figure 1B). The targets associated with CKD were found to be 3704. A Venn diagram was generated to delve into the potential targets of SQSKG in treating CKD, illustrating 149 common targets considered as possible targets of SQSKG against CKD (Figure 1C and Table S2). Besides, the PPI network comprised 149 nodes and 2806 edges, with an average node degree of 38.2 (Figure 1D). The top 10 targets were identified based on their MCC score (Figure 1E). A network connecting key compounds and common targets was also constructed (Figure 1F), revealing 49 key compounds associated with the 149 targets, detailed in Table S3. The top 6 compounds, ranked by degree value, included quercetin, luteolin, kaempferol, ellagic acid, atractylenolide II, and stigmasterol.

KEGG pathway enrichment analysis was performed based on the 149 common targets and identified 148 pathways (Table S4), from which the top 25 pathways were extracted and presented in bar charts and a Sankey diagram based on P values (Figure 2A and B). The primary pathways are cancer, PI3K/AKT, Rap1, MAPK, and HIF-1 signaling. Additionally, GO analysis revealed that BP terms were mainly associated with protein phosphorylation, cell activation, cell migration, and inflammatory and oxidative stress responses. The CC terms were distributed in the membrane and receptor complex, while MF terms were linked to kinase activity and protein binding (Figure 2C–E and Table S5). To further unveil the potential mechanism of SQSKG against CKD, a target-pathway network was constructed based on the top 10 signaling pathways and their corresponding targets (Figure 2F). Enrichment analysis highlighted the PI3K/AKT signaling pathway in SQSKG's treatment of CKD. A subnet extraction focusing on the relationship between SQSKG and the PI3K/AKT pathway revealed 26 involved targets, with the top five being AKT1, MAPK1, EGFR, HSP90AA, and IGF1R (Figure 2G).

Verification of the Interaction via Molecular Docking

Before conducting molecular docking analysis, ten targets in the PPI network were selected based on their node degree, MCC score, and relevance to the PI3K/AKT pathway. Then, we ranked the compounds in the compound-target network (Figure 1F and

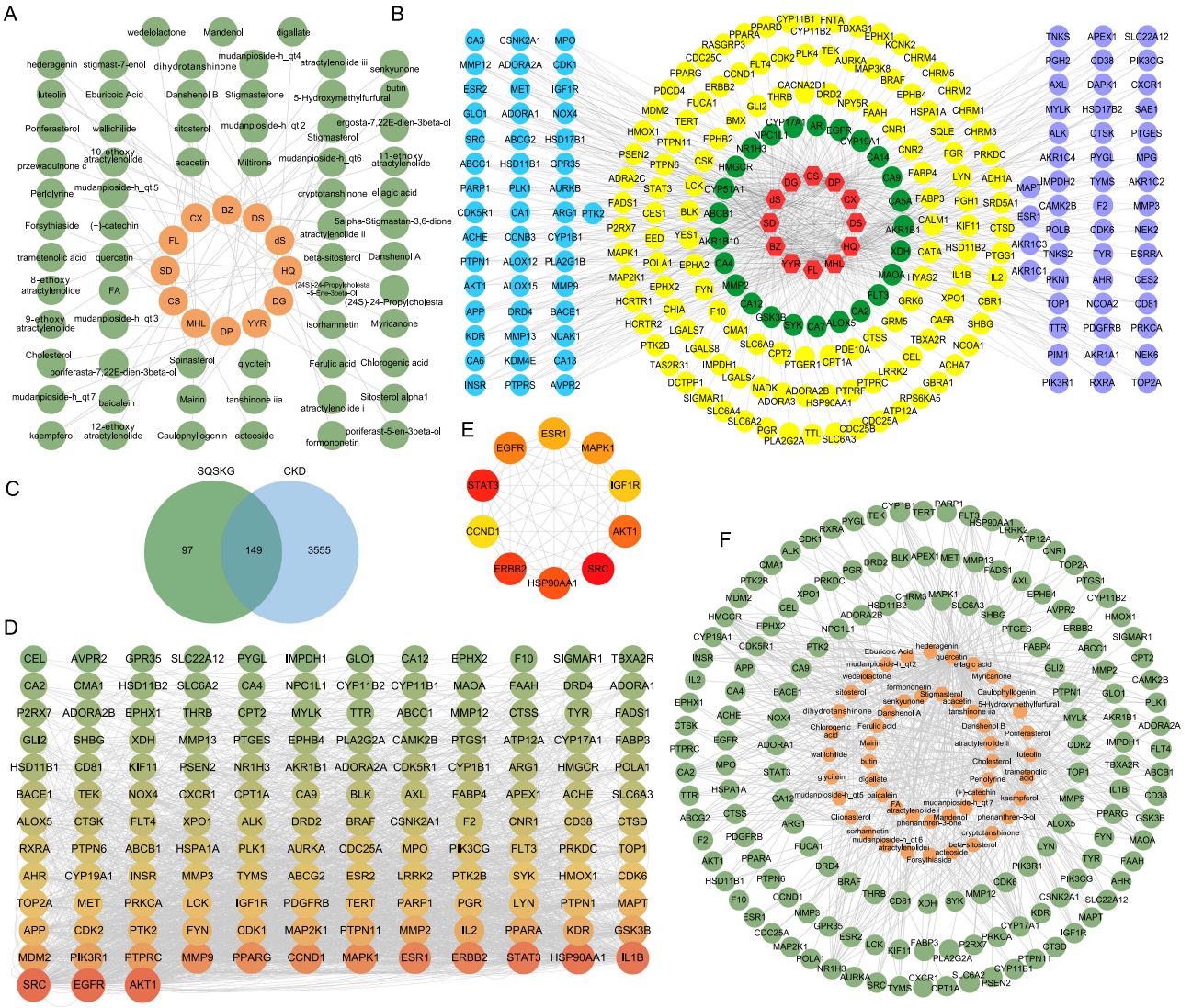

Figure 1 Compounds and targets collection. (**A**) Network of 12 herb medicines and 64 key compounds in Shenqi Shenkang granule (SQSKG). (**B**) Herb-target network of SQSKG. Red hexagons represent 12 herb medicines, and colorful round nodes represent target groups shared by different amounts of herbs. Green nodes (n=23) are the common target proteins shared by more than six herbs. Left Blue nodes (n=47) are the targets that 4 or 5 herbs contain. Right Purple nodes (n=44) represent the targets that 2 or 3 herbs shared. Yellow nodes (n=126) stand for the unique targets that only one herb contains. Targets analysis of SQSKG and chronic kidney disease (CKD). (**C**) Venn diagram of overlapping genes of SQSKG and CKD. (**D**) PPI network (149 nodes and 2806 edges) of SQSKG targets against CKD targets. The node size and color are proportional to the degree values. (**E**) The top 10 high-relevant targets were screened according to their MCC score. (**F**) Network of 149 Common targets and 49 correspondent compounds.

Table S3) according to their degree value. To ensure diversity, we selected the compound with the highest degree value from each class, leading to a final selection of the top 10 compounds for molecular docking. The analysis was then performed to evaluate the binding energy of the selected compound-target interactions. As shown in Figure 3A, the top three compounds of the top five proteins were as follows: PI3K to Quercetin (−9.12 kcal/mol), stigmasterol (−7.82 kcal/mol), and Wallichilide (−7.43 kcal/mol). AKT1 to Wallichilide (−7.36 kcal/mol), Stigmasterol (−6.79 kcal/mol), and Quercetin (−6.56 kcal/mol). mTOR to Stigmasterol (−6.97 kcal/mol), Wallichilide (−6.64 kcal/mol), and Atractylenolide ii (−6.33 kcal/mol). STAT3 to Stigmasterol (−7.73 kcal/mol), Atractylenolide ii (−6.51 kcal/mol), and Luteolin (−5.14 kcal/mol). EGFR to Stigmasterol (−7.22 kcal/mol), Atractylenolide ii (−7.06 kcal/mol), and Quercetin (−6.93 kcal/mol). Therefore, based on the binding energy between compounds and targets, the top three compounds most relevant to the PI3K/AKT/mTOR pathway are quercetin, stigmasterol, and atractylenolide II. Furthermore, 3D and 2D ligand-protein interaction diagrams for six compound-target complexes were displayed in Figure 3B.

https://doi.org/10.2147/DDDT.S513824

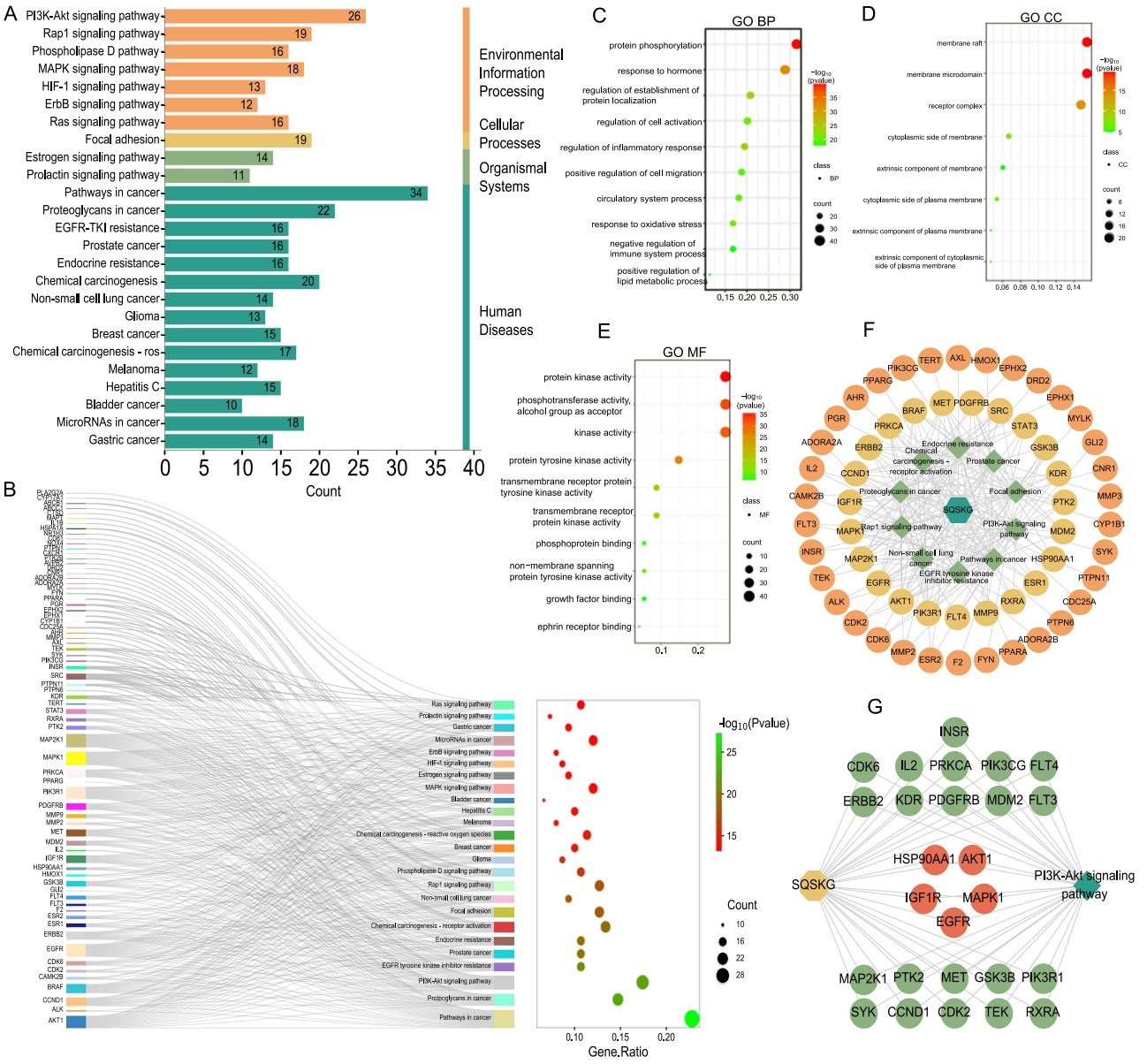

Figure 2 Enrichment analysis of the common targets. (**A**) Top 25 significantly enriched terms in KEGG pathways. (**B**) KEGG pathway Sankey diagram. (**C**–**E**) GO analysis of the common targets. (**F**) Target-pathway network of Shenqi Shenkang granule (SQSKG) against chronic kidney disease (CKD). (**G**) The SQSKG targets enrichment in the PI3K-AKT signaling pathway.

Abbreviations: BP, biological process; MF, molecular function; CC, cellular component.

Determination of the Main Bioactive Compounds of SQSKG

For quality control, Vanquish UHPLC™ identified 54 chemical components in SQSKG. The total ion chromatogram (TIC) is shown in Figure S1, and 15 representative compounds are displayed in Table 2. The detailed results are provided in Table S6. The primary compounds matched those identified as key by network pharmacology. Therefore, the Vanquish UHPLC™ results can effectively control the quality of SQSKG.

SQSKG Improved HK-2 Cell Viability

A colony formation assay was employed to assess cell survival rates. As illustrated in Figure 4A and B, colony counts increased following exposure to SQSKG compared to the Vehicle group. To examine the cell migration rate of HK-2 cells, a wound-healing assay was conducted after treatment with or without SQSKG (100 μg/mL) for 12 or 24 hours. As depicted in Figure 4C and D, HK-2 cells exhibited an accelerated migration rate after exposure to SQSKG compared to

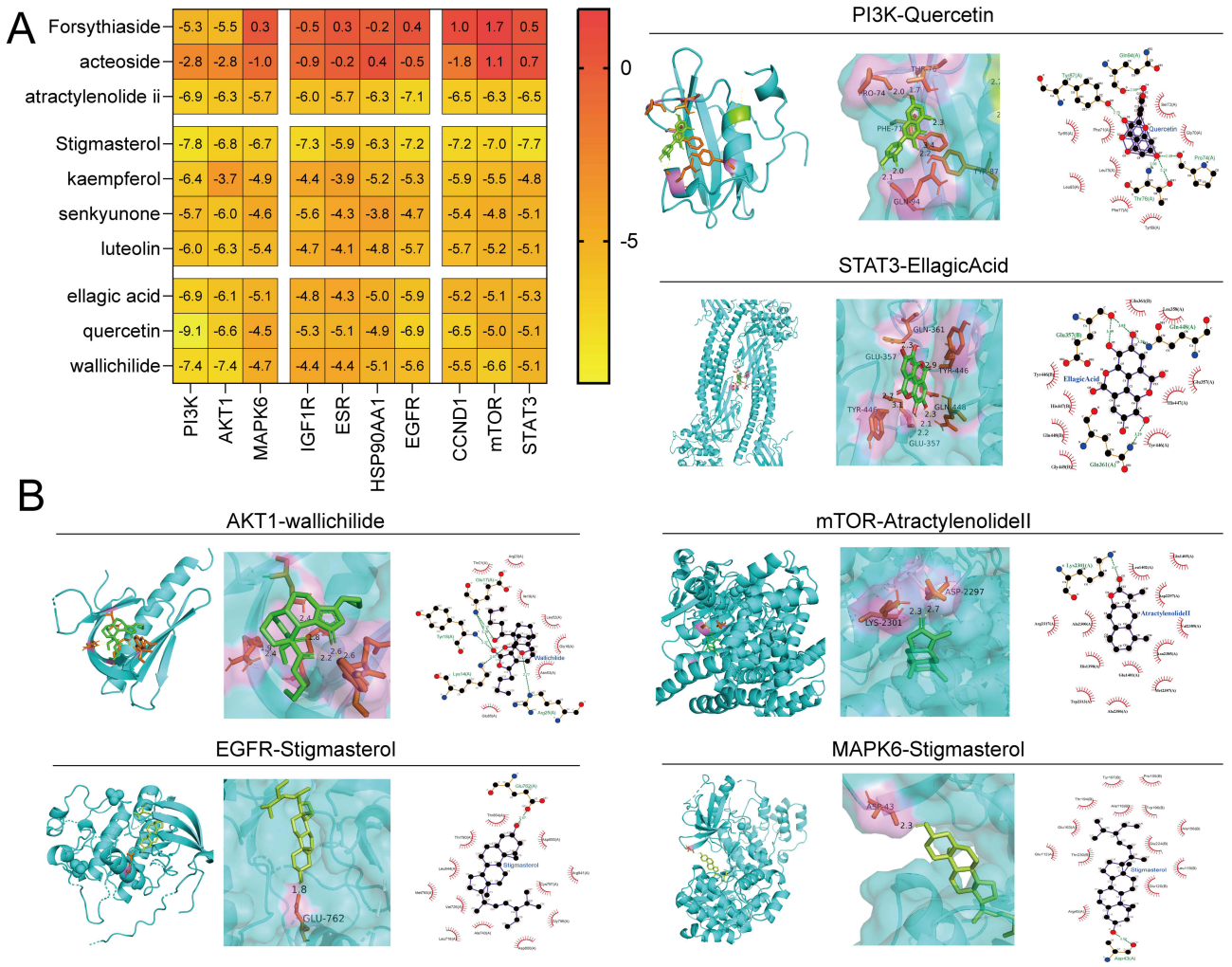

Figure 3 Molecular docking results. (**A**) The heatmap of the binding energy of 10 key targets to 10 compounds in Shenqi Shenkang granule (SQSKG). (**B**) The representative docking complex of SQSKG compounds and core targets.

the Vehicle group. Additionally, the CCK-8 assay showed that the survival rate of HK-2 cells increased gradually with higher concentrations of SQSKG and prolonged exposure time (Figure 4E). The influence of SQSKG on HK-2 cells exposed to AGE-BSA was also evaluated (Figure 4F), showing that SQSKG improved the viability of HK-2 cells exposed to AGE-BSA in a concentration-dependent manner. Furthermore, as displayed in Figure 4G and H, the AGE-BSA group exhibited elevated MDA levels (a byproduct of ROS) and reduced SOD levels (a ROS scavenger) compared to the Vehicle group. However, SQSKG treatment significantly reduced MDA levels and increased SOD levels compared to the AGE-BSA group.

SQSKG Alleviated Cell Fibrosis Suppressing the PI3K/AKT/mTOR Pathway

The regulatory effects of SQSKG on cell fibrosis and the PI3K/AKT/mTOR pathway were investigated through Western blot and immunofluorescence assays. As depicted in Figure 5A, the ratio of phosphorylated proteins (p-PI3K, p-Akt, p-mTOR) to their total protein counterparts (PI3K, Akt, mTOR) was significantly elevated in the AGE-BSA group compared to the Vehicle group. This ratio decreased in the SQSKG group relative to the AGE-BSA group, with a more pronounced reduction observed at higher SQSKG concentrations. To further explore SQSKG's impact on cell fibrosis and apoptosis, we analyzed the expression of key fibrosis-related proteins (TGF-β, α-SMA) and apoptosis-related proteins (Bax, caspase-3). As shown in Figure 5B, the levels of TGF-β, α-SMA, Bax, and caspase-3 were increased in the AGE-BSA group but decreased in the SQSKG group. Notably, a significant reduction was observed at the higher

https://doi.org/10.2147/DDDT.S513824

Table 2 Fifteen Representative Compounds Identified by Vanquish UHPLC™

NO.	$RT_{[min]}$	Calc. MW	m/z	Formula	ppm	ms2Adduct	Compounds
1	0.60	122.12	123.06	C6H6N2O	2.17	[M+H]+	Nicotinamide
2	0.87	166.17	167.07	C9H10O3	1.50	[M+H]+	Paeonol
3	1.05	302.24	303.05	C15H10O7	0.49	[M+H]+	Quercetin
4	1.34	446.40	447.13	C22H22O10	0.46	[M+H]+	Calycosin-7-O-beta-D-glucoside
5	1.52	308.26	301.03	C15H8O7	2.13	[M+H]+	Demethylwedelolactone
6	1.54	286.24	287.06	C15H10O6	0.72	[M+H]+	Kaempferol
7	2.42	302.19	303.01	C14H6O8	1.10	[M+H]+	Ellagic acid
8	2.50	286.24	287.06	C15H10O6	1.10	[M+H]+	Luteolin
9	2.88	138.12	139.04	C7H6O3	1.01	[M+H]+	Salicylic acid
10	3.02	396.40	414.21	C20H28O8	0.93	[M+NH4]+	Lobetyolin
11	4.29	468.70	455.35	C30H46O3	0.43	[M+H]+	Dehydrotrametenolic acid
12	5.87	785.00	785.47	C41H68O14	0.71	[M+H]+	Astragaloside IV
13	7.67	230.30	231.14	C15H18O2	0.50	[M+H]+	Atractylenolide I
14	9.01	380.50	381.21	C24H28O4	1.78	[M+H]+	Levistilide A
15	10.23	294.30	295.13	C19H18O3	0.67	[M+H]+	Tanshinone IIA

SQSKG dose (100 μg/mL) compared to the AGE-BSA group. Additionally, immunofluorescence analysis presented in Figure 5C and D demonstrated that SQSKG reduced TGF-β expression in HK-2 cells exposed to AGE-BSA. These findings suggest that SQSKG may mitigate fibrosis in HK-2 cells exposed to AGEs by inhibiting the PI3K/AKT/mTOR pathway.

SQSKG Activated Autophagy Pathway in HK-2 Cells

To investigate the effect of SQSKG on autophagy, HK-2 cells were infected with Ad-mCherry-GFP-LC3B adenovirus to observe the autophagy flux (Figure 6A). After infecting cells with Ad-mCherry-GFP-LC3B adenovirus, mCherry-GFP-LC3B shows diffuse yellow fluorescence (a combined effect of mCherry and GFP) in the cytoplasm under non-autophagic conditions. Under autophagic conditions, it forms yellow puncta (LC3 dots) on autophagosome membranes. When autophagosomes fuse with lysosomes, partial quenching of the GFP fluorescence results in red dots, indicating efficient autophagy flux. As shown in Figure 6B and C, under the basal level of autophagy in the Vehicle group, the cytoplasm exhibited diffused yellow fluorescence. After AGE-BSA exposure for 24 h, this fluorescence transformed into aggregated yellow dots, indicating autophagy progress. However, mainly yellow rather than red dots increased in the cells, suggesting that many autophagosomes were not degraded by lysosomes. SQSKG treatment promoted autophagosome-lysosome fusion, resulting in partial quenching of GFP fluorescence and the appearance of red dots, indicating enhanced autophagosome degradation (Figure 6D). Additionally, the AGE-BSA group showed a slightly higher number of dots than the Vehicle group, and SQSKG intervention further increased the dot count. The result was consistent with the Western Blot analysis. Figure 6E showed the expression level of LC3B-II (a structural protein of autophagosomes) was slightly accumulated after AGE- BSA exposure and substantially increased in the SQSKG group. To further determine whether the accumulation of LC3B-II indicates autophagic activation or impaired degradation, we investigated the autophagy substrate p62. As shown in Figure 6E and F, both Western Blot analyses and immunofluorescence confirmed increased p62 expression in HK-2 cells exposed to AGE-BSA. Therefore, LC3B-II accumulation is most likely a result of dysfunctional autophagosome degradation. Moreover, the AGE-BSA group exhibited downregulated Beclin-1 levels and a decreased LC3B-II/LC3B-I ratio, confirming autophagic induction inactivation (Figure 6E). This effect was likely attributed to the upregulation of the PI3K/AKT/mTOR pathway. However, SQSKG treatment reversed these expressions by suppressing the PI3K/AKT/mTOR pathway and subsequentially increased the number of autophagic vesicles, as evidenced by elevated LC3B-II levels. The data suggest that SQSKG not only promoted autophagy induction by inhibiting the PI3K/AKT/mTOR pathway but also restored abnormal degradation in the downstream autophagic process.

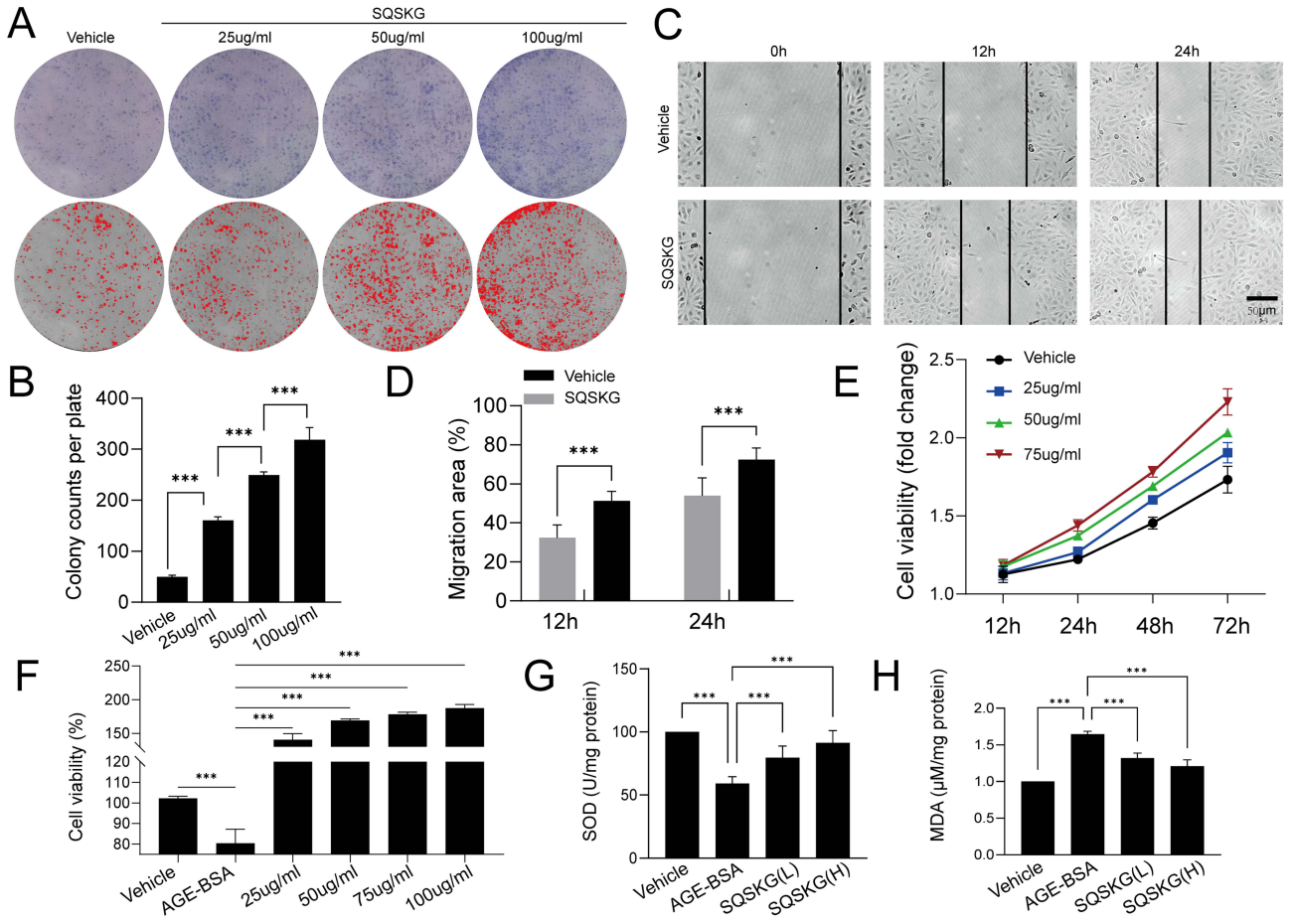

Figure 4 Effect of Shenqi Shenkang granule (SQSKG) on HK-2 cell proliferation and cellular oxidative stress. (**A**) Colony formation assay of HK-2 cells exposed to SQSKG. (**B**) Quantitative analysis of colony formation assay (n = 6). (**C**) Wound-healing assay of HK-2 cells after exposure to SQSKG (100 μg/mL). Scale bar, 50 μm. (**D**) Quantitative analysis of wound-healing assay (n = 6). (**E**) Cell viability assay of HK-2 cells under different concentrations of SQSKG (n = 6). (**F**) Effects of different concentrations of SQSKG on AGE-BSA (100 μg/mL) treated HK-2 cells (n = 6). (**G** and **H**) Superoxide dismutase (SOD) and Malondialdehyde (MDA) levels in each group (n = 6). SQSKG(L/H): AGE-BSA (100 μg/mL) plus SQSKG (50/100 μg/mL). ***, $p < 0.001$.

SQSKG Improved the Mitochondria Function and Morphology of HK-2 Cells

JC-1 probe was used to detect mitochondrial membrane potential (MMP). JC-1 forms red aggregates at high MMP and green monomers at low MMP. In Figure 7A and B, HK-2 cells exposed to AGE-BSA showed increased green monomers and decreased red aggregates, which were reversed by SQSKG treatment. The reduced red-to-green fluorescence ratio in the AGE-BSA group was increased by SQSKG (Figure 7C), indicating SQSKG's protective effect on MMP. Additionally, Figure 7D and E showed that SQSKG reduced the high ROS fluorescence intensity caused by AGE-BSA. Mitochondrial morphology was evaluated using Mito-Tracker Green and analyzed with ImageJ, determining size by area and perimeter, and shape by form factor (FF) and aspect ratio (AR). The mitochondrial network's complexity was assessed by branch and junction counts, branch length, and mean branch length. In Figure 7F, mitochondria in the Vehicle group displayed a highly connected, filamentous morphology, while HK-2 cells exposed to AGE-BSA for 24 hours had small, round mitochondria with limited branching. Cells treated with SQSKG maintained mitochondrial integrity despite AGE-BSA damage. Quantitative analysis confirmed these findings from various perspectives (Figure 7G and H).

SQSKG Improved Renal Function and Morphology

An in vivo adenine-induced CKD model was used to investigate SQSKG's effect on renal fibrosis. As shown in Figure 8A, the procedure was followed, and Figure 8B demonstrated that SQSKG mitigated kidney fibrosis in a concentration-dependent manner. Serological assays showed that SQSKG improved renal function by reducing high

https://doi.org/10.2147/DDDT.S513824

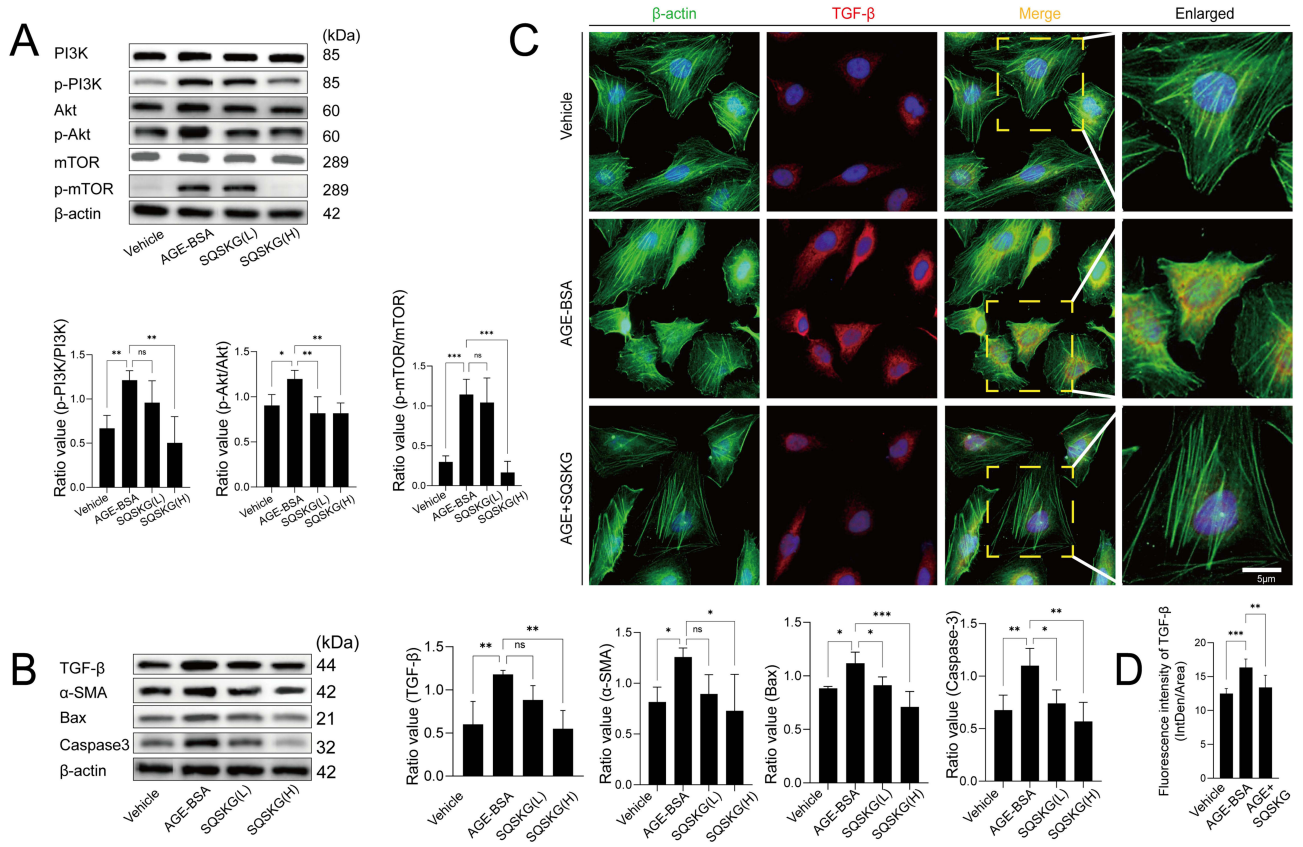

Figure 5 Effects of Shenqi Shenkang granule (SQSKG) on the PI3K/AKT/mTOR pathway, fibrosis, and apoptosis in HK-2 cells exposed to AGE-BSA. (**A** and **B**) Western blot and quantification of the relative expressions of PI3K, p-PI3K, AKT, p-AKT, mTOR, p-mTOR, TGF-β, α-SMA, Bax, and caspase-3 in each group (n = 6). SQSKG(L/H): AGE-BSA (100 μg/mL) plus SQSKG (50/100 μg/mL). (**C** and **D**) Immunofluorescence staining and quantification of transforming growth factor-beta (TGF-β) expression in each group (n = 6). The dotted yellow boxes indicate the enlarged regions of the immunofluorescence images. Scale bar, 5 μm. *, $p < 0.05$; **, $p < 0.01$; ***, $p < 0.001$; ns, not significant.

levels of SCR, BUN, and 24-hour urine albumin in CKD animals (Figure 8C). Furthermore, histological staining revealed significant pathology in the CKD group, including diffused glomerulosclerosis, interstitial fibrosis, arteriolosclerosis, inflammatory cell infiltration, and tubular dilation. These pathological features were noticeably alleviated by SQSKG in a dose-dependent manner (Figure 8D–G). The effects of SQSKG were comparable to valsartan, with SQSKG showing a more significant reduction in renal fibrosis.

SQSKG Alleviated Renal Fibrosis and Activated Autophagy

To observe the anti-fibrotic effects of SQSKG, fibrosis-related proteins were analyzed using histological staining and Western blot. Consistent with the results of Masson's staining, SQSKG reversed the adenine-induced accumulation of Col-I, α-SMA, and TGF-β (Figure 9). Given TGF-β's crucial role in renal fibrosis and its link to autophagy, we further examined autophagy in the adenine-induced CKD model. As shown in Figure 10, the CKD group exhibited increased levels of LC3 and p62, indicating either adaptive autophagy activation or impaired autophagosome degradation. However, SQSKG treatment led to an increase in LC3 puncta and a reduction in p62 expression in the kidneys. This suggests that the observed increase in autophagosomes in the CKD model may represent a protective stress response, although it was insufficient to sustain cellular metabolism. Notably, SQSKG enhanced this insufficient self-protective response to eliminate abnormal organelles or proteins. These findings suggest that SQSKG may alleviate renal fibrosis by activating autophagy.

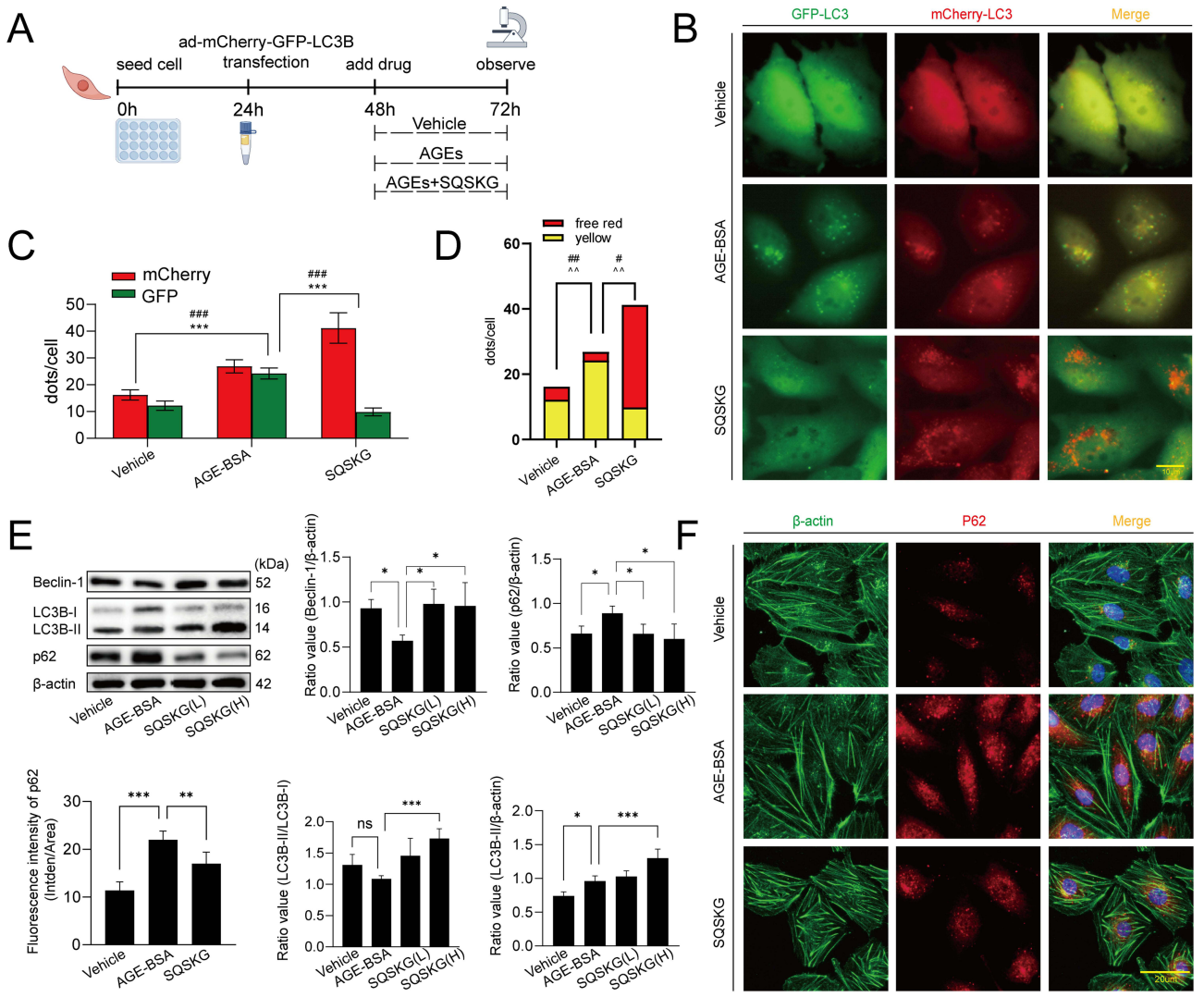

Figure 6 Effects of Shenqi Shenkang granule (SQSKG) on the autophagy-lysosome pathway activity in HK-2 cells exposed to AGE-BSA. (**A**) Schematic diagram of the experimental procedure of ad-mCherry-GFP-LC3B transfection. (**B**) Fluorescence staining of HK-2 cells transfected with ad-mCherry-GFP-LC3B fusion protein and treated with Vehicle (culture medium), AGE-BSA (100 μg/mL), and AGE-BSA plus SQSKG (100 μg/mL) for 24 h. Scale bar, 10 μm. (**C**) The ratio of yellow or free red puncta per cell in (**B**). (**D**) Quantification of green or red puncta per cell in (**B**) (n = 6). (**E**) Western blot and quantification of Beclin-1, LC3B-II/I, and p62 in each group (n = 6). (**F**) Immunofluorescence analysis of p62 expression in each group (n = 6). Scale bar, 20 μm. SQSKG(L/H): AGE-BSA (100 μg/mL) plus SQSKG at lower (50 μg/mL) or higher (100 μg/mL) doses. *, $p < 0.05$; **, $p < 0.01$; ***, $p < 0.001$; #, $p < 0.05$ (for red or free red puncta); ##, $p < 0.01$; ###, $p < 0.001$; ^^, $p < 0.01$ (for yellow puncta); ns, not significant.

Discussion

Chronic kidney disease typically progresses slowly over time. Based on the TCM theory, we optimized the classic formula Shenqi Dihuang Decoction into Shenqi Shenkang Granule, which has been clinically proven to improve renal function effectively and has received approval from the local Medical Products Administration9. Hence, it is necessary to clarify the practical mechanisms of SQSKG. In this study, we employed network pharmacology, molecular docking, and experiments (in vitro and in vivo) to explore the mechanisms of SQSKG.

Network pharmacology analysis confirmed that the PI3K/AKT pathway is the most relevant for treating CKD with SQSKG, with quercetin, stigmasterol, and atractylenolide II identified as the top three key compounds. Therefore, to further confirm the bio-activeness of SQSKG and its regulatory effect on the PI3K/AKT/mTOR pathway, we conducted a series of experiments based on human renal tubular epithelial cells HK-2. Firstly, as the results have manifested, SQSKG promoted HK-2 cell proliferation and migration, consistent with the GO analysis. In addition, KEGG analysis revealed that AGE-RAGE signaling, a crucial factor in the development of CKD secondary to diabetic kidney disease,

https://doi.org/10.2147/DDDT.S513824

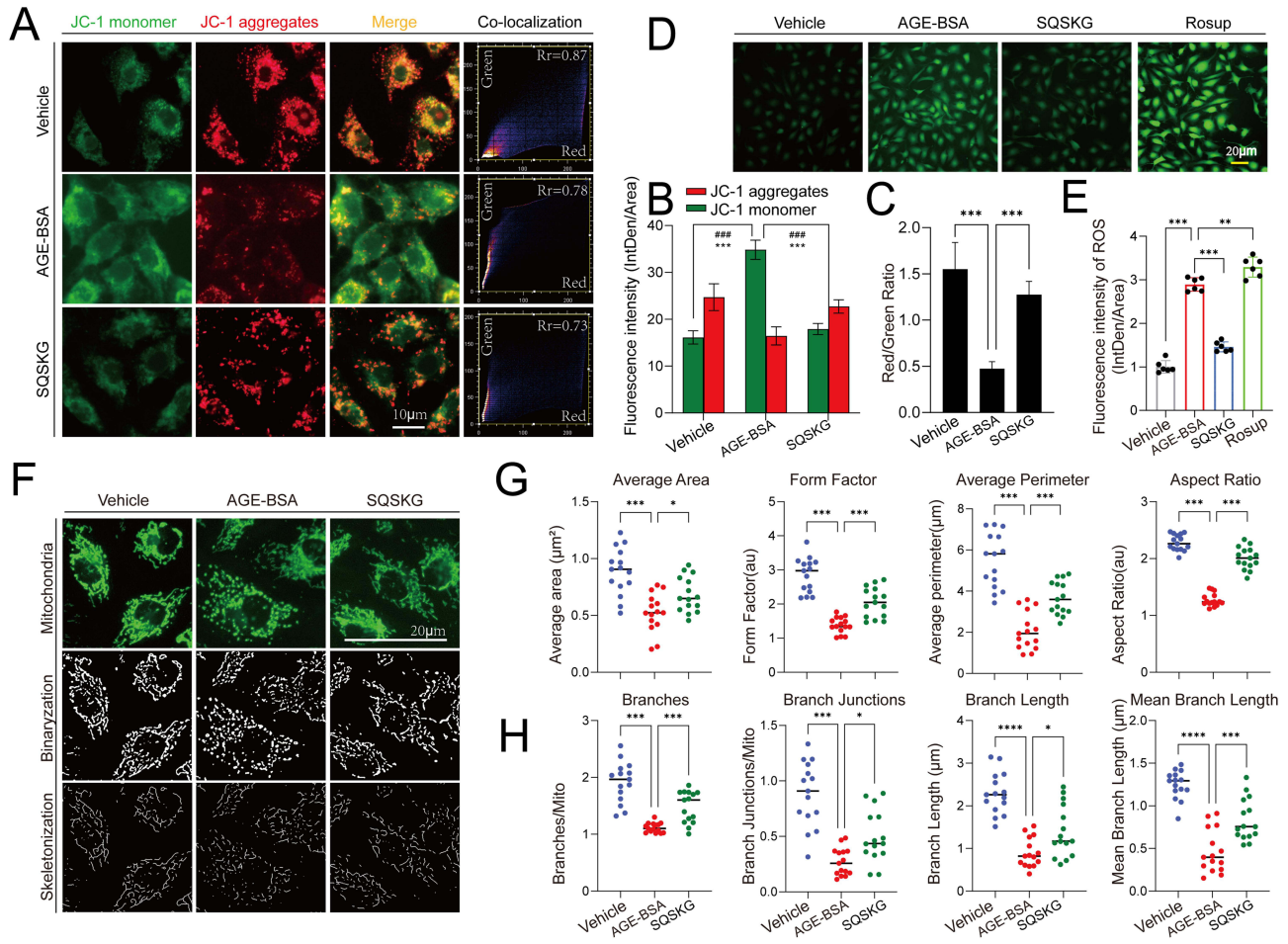

Figure 7 Effect of Shenqi Shenkang granule (SQSKG) on mitochondria and reactive oxygen species (ROS) in HK-2 cells exposed to AGE-BSA. (**A**) Fluorescent analysis of mitochondrial membrane potential of HK-2 cells treated separately with Vehicle (culture medium), AGE-BSA (100 μg/mL), and AGE-BSA plus SQSKG (100 μg/mL) for 24 h. Scale bar, 10 μm. (**B** and **C**) Quantitative data for green and red puncta and the red/green ratio (n = 6). ###, $p < 0.001$ (for green puncta); ***, $p < 0.001$ (for red puncta and red/green ratio); (**D** and **E**) Fluorescent analysis and quantification of ROS (n = 6). Scale bar, 20 μm. (**F**) Fluorescent analysis of mitochondrial morphology and binarization and skeletonization images. Scale bar, 20 μm. (**G** and **H**) Quantitative data of mitochondrial morphological parameters (n = 15). *, $p < 0.05$; **, $p < 0.01$; ***, $p < 0.001$; ****, $p < 0.0001$.

was involved in the treatment. We conducted a cell viability assay to test the influence of SQSKG on HK-2 cells exposed to AGEs. We discovered that SQSKG was beneficial to the proliferation of HK-2 cells under AGE pressure. As a result, we decided to utilize AGEs as stimuli on HK-2 cells to investigate the protective effects of SQSKG against AGE-induced damage and its potential mechanisms for preventing the progression of CKD.

As it is well known, AGEs are molecules formed by the non-enzymatic glycation of proteins, lipids, and nucleic acids.[26] Evidence suggests that AGEs can activate the PI3K/AKT/mTOR pathway, leading to fibrosis and apoptosis in different tissues, including the kidneys.[27,28] The results of this study also showed that AGEs activated the protein phosphorylation of PI3K, AKT, and mTOR in HK-2 cells, resulting in the accumulation of TGF-β, α-SMA, Bax, and caspase-3 which were important proteins related to fibrosis and apoptosis. However, since the PI3K/AKT/mTOR pathway plays a crucial role in regulating cell growth, survival, metabolism, and proliferation,[29] it is intriguing that the viability of HK-2 cells was inhibited after exposure to AGE-BSA despite the increased level of p-PI3K, p-AKT, and p-mTOR. After reviewing the literature, we hypothesized that several possible reasons could explain this discrepancy.

On the one hand, dysregulation or prolonged activation of the PI3K/AKT/mTOR pathway can lead to increased production of pro-fibrotic factors and the excessive accumulation of extracellular matrix (ECM) proteins.[29,30] On the other hand, the excessive accumulation of misfolded proteins and injured organelles cannot be cleared by inactivated autophagy induced by excessive activation of mTOR and the impaired autophagy-lysosome pathway resulting from

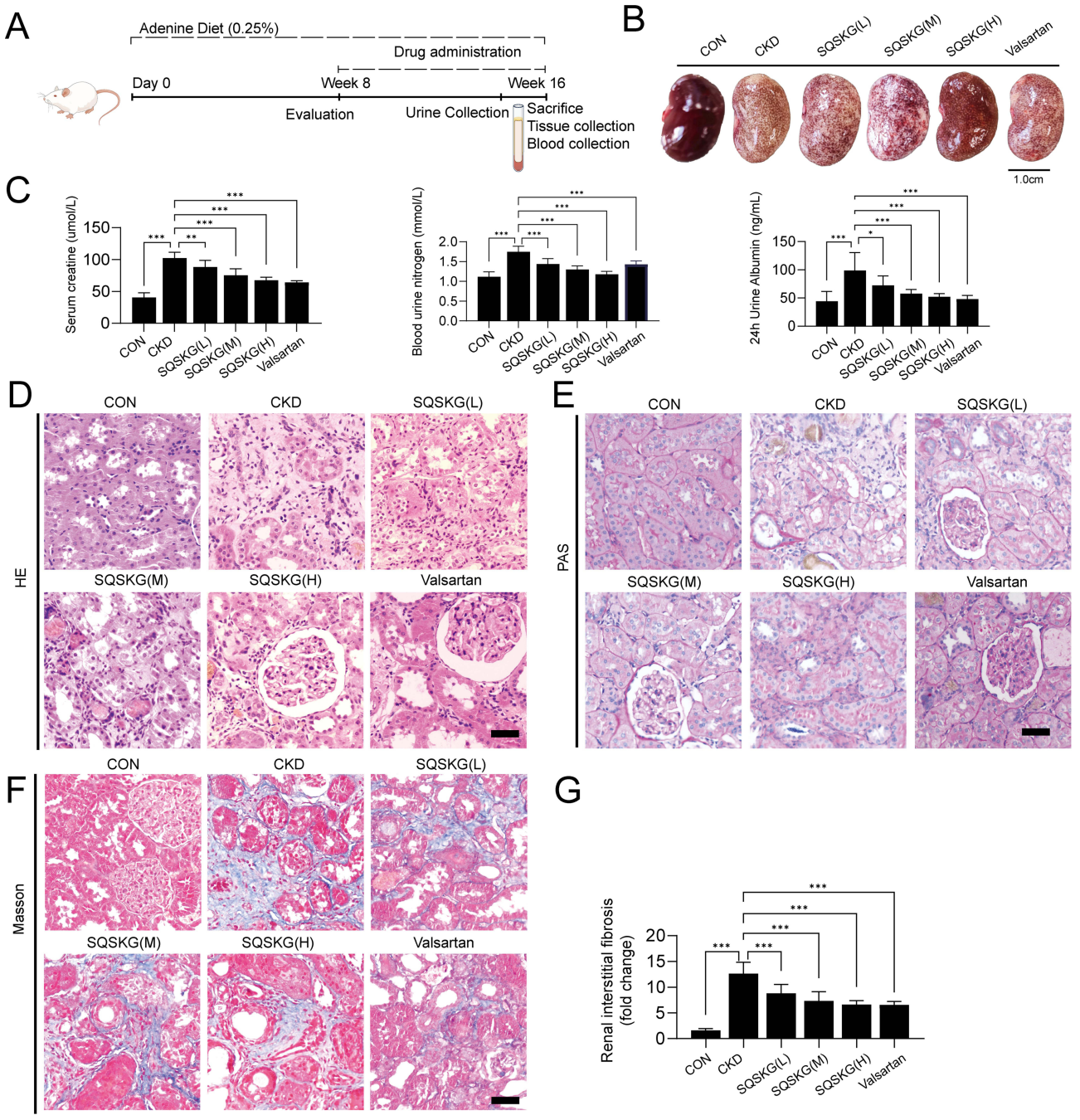

Figure 8 Effects of Shenqi Shenkang granule (SQSKG) in an adenine-induced chronic kidney disease (CKD) animal model. (**A**) Schematic representation of the experimental procedure. (**B**) Representative images of kidneys from different experimental groups. Scale bar, 1.0 cm. (**C**) Serological parameters and renal fibrosis rate in different groups (n = 10). (**D**–**F**) Representative images of Hematoxylin-eosin (H&E), periodic acid-Schiff (PAS), and Masson's trichrome staining of renal tissues. Scale bar, 20 μm. (**G**) Semiquantitative assessment of renal interstitial fibrosis based on Masson staining images (n = 5). *, $p < 0.05$; **, $p < 0.01$; ***, $p < 0.001$.

AGEs-induced lysosome membrane permeabilization (LMP).[31–33] Hence, since KEGG analysis also revealed autophagy as one of the pathways implicated in CKD treatment by SQSKG, further investigation was performed to verify the hypothesis.

Autophagy is reported to play a complex role in the kidney under different contexts.[34,35] Adaptive autophagy suppresses renal fibrosis in certain conditions, but impaired or dysregulated autophagy might be associated with fibrotic disorders.[36] In our study, AGEs reduced the Beclin-1 and LC3-II/LC3-I ratio expression in HK-2 cells, which might be attributed to high-rising p-mTOR. mTOR is a protein kinase that inhibits autophagy by phosphorylating and inhibiting

https://doi.org/10.2147/DDDT.S513824

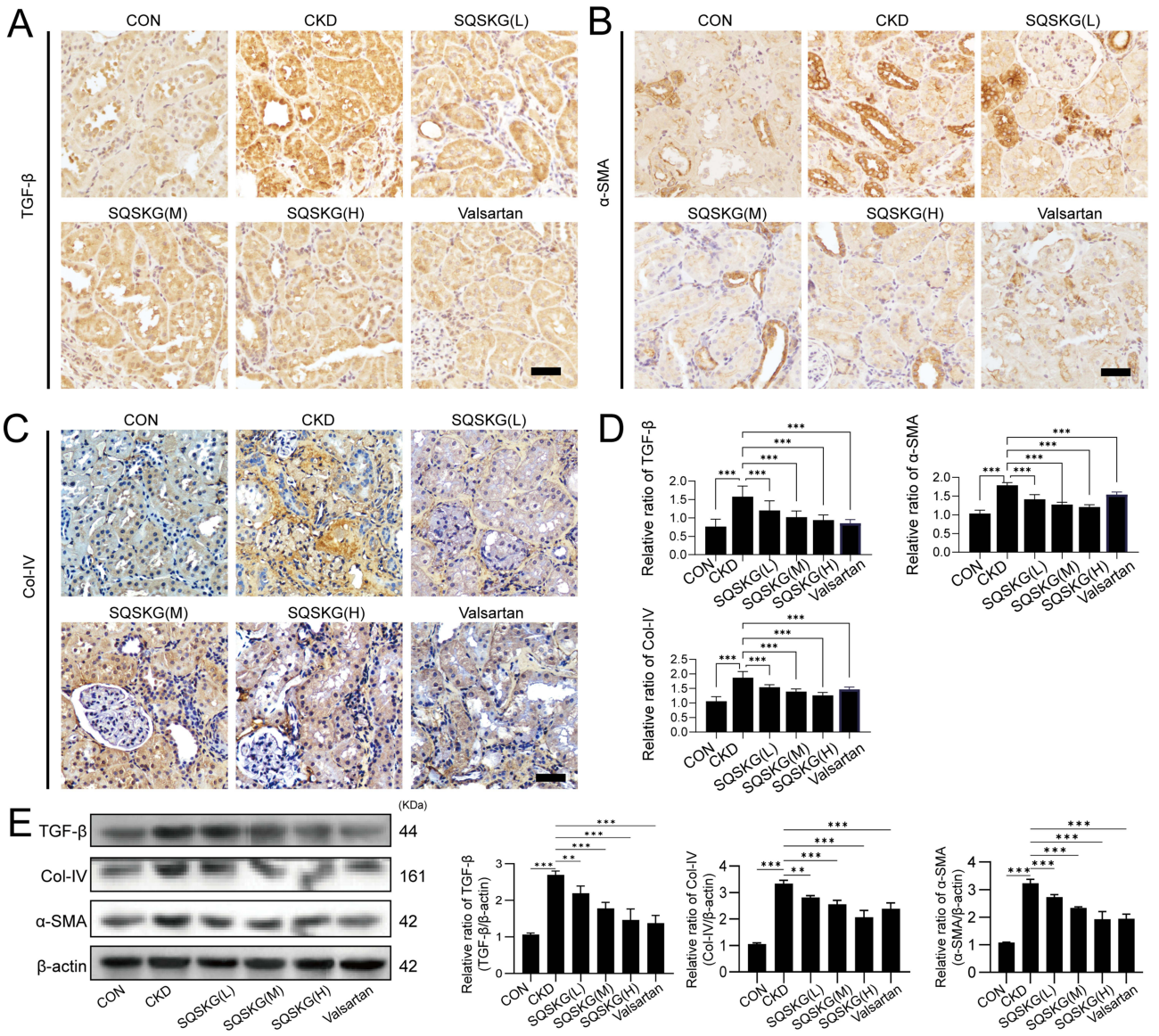

Figure 9 Antifibrotic effects of Shenqi Shenkang granule (SQSKG) in an adenine-induced chronic kidney disease (CKD) animal model. (**A–D**) Immunohistochemical staining and quantitative analysis of renal fibrosis markers, including transforming growth factor-beta (TGF-β), alpha-smooth muscle actin (α-SMA), and collagen IV (Col-IV) (n = 5). Scale bar, 20 μm. (**E**) Western blot analysis and quantification of TGF-β, α-SMA, and Col-IV expression in renal tissues (n = 6). **, $p < 0.01$; ***, $p < 0.001$.

the activity of Beclin-1, which is crucial in recruiting LC3-I to form LC3-II to nucleate the autophagosome membrane.[37,38] As per the results, SQSKG induced autophagy in AGEs-injured HK-2 cells by suppressing the phosphorylation level of the PI3K/AKT/mTOR pathway.

Meanwhile, another confusing finding was that a slightly increased LC3-II puncta level was observed in AGE-exposure cells despite the reduced Beclin-1 and LC3-II/LC3-I ratio levels. On this account, the ad-mCherry-GFP-LC3B protein was applied to investigate the autophagic flux by detecting the fusion level of autophagosome and lysosome. The results demonstrated that the slight LC3-II accumulation was attributed to the destructed fusion process of autophagosome and lysosome resulting from AGE damage, consistent with the literature.[31] As the results manifested, the effect of SQSKG on reducing p62 is most likely associated with enhancing the cleaning ability of autophagy by promoting the fusion process of the two critical cellular organelles. Hence, our finding indicated that SQSKG promoted autophagic induction by increasing LC3-II level and promoted autophagosome degradation by improving the autolysosome fusion rate, which was confirmed by the decreased level of p62.

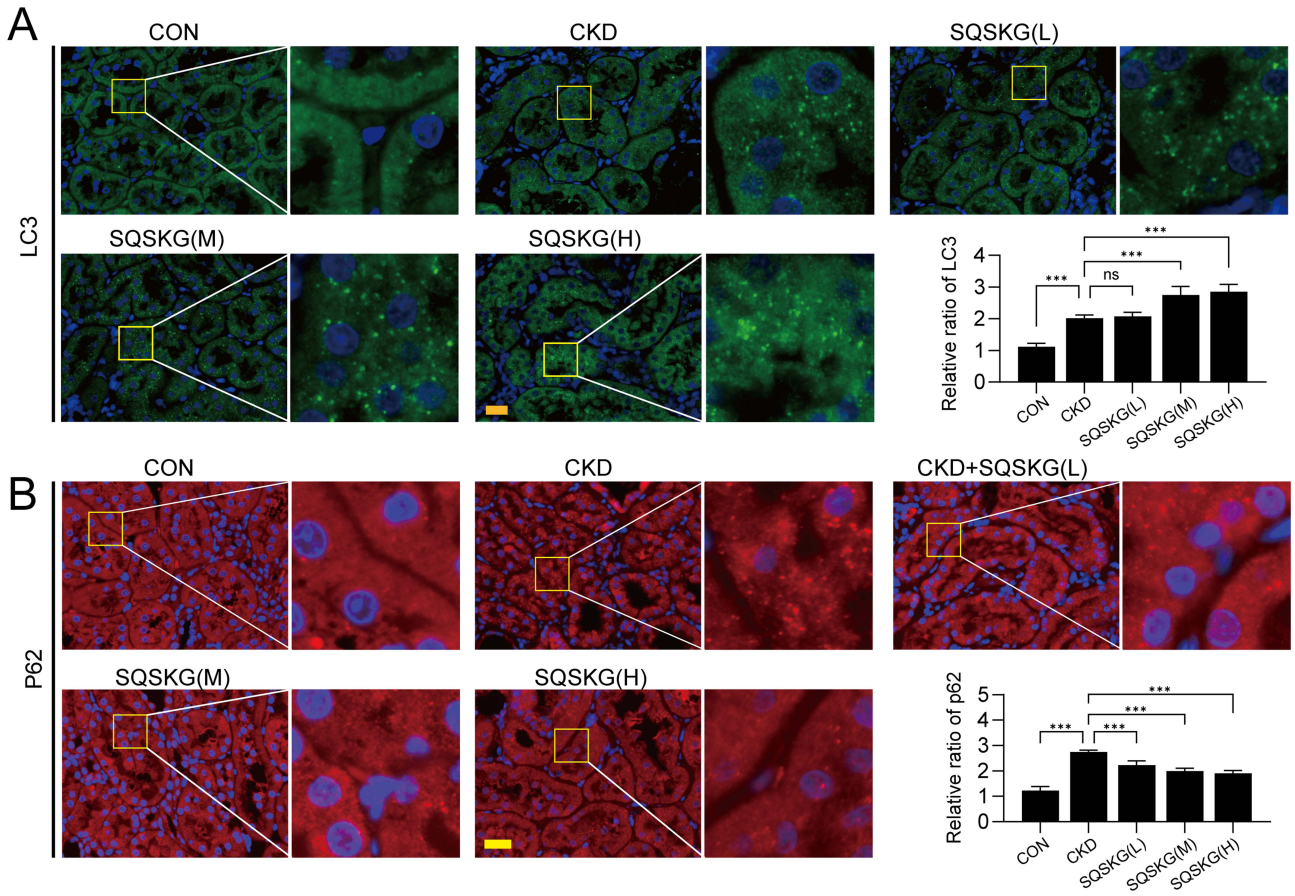

Figure 10 Effects of Shenqi Shenkang granule (SQSKG) on the expression of autophagy-related proteins LC3 and p62 (n = 5). (**A**) Immunofluorescence staining and quantitative analysis of the autophagy markers LC3 in renal tissues. Scale bar, 20 μm. (**B**) Immunofluorescence staining and quantitative analysis of p62 in renal tissues. Scale bar, 20 μm. ***, $p < 0.001$; ns, not significant.

The fusion dysfunction of autophagosomes and lysosomes has been linked to lysosomal impairment caused by AGEs-RAGE axis-mediated oxidative stress.[31] AGEs activate RAGE, promoting excessive ROS generation within abnormal mitochondria.[39,40] This oxidative stress, in turn, further damages mitochondrial structures, impairing their function and integrity.[41,42] Mitochondria are dynamic organelles undergoing continuous fusion and fission,[43] and healthy mitochondria form mobile, tubular networks in cells. In contrast, stressed cells often exhibit swollen and fragmented mitochondria.[44] Our study demonstrated that SQSKG aids in restoring mitochondrial function and morphology, as evidenced by improved MMP and mitochondrial integrity. This beneficial effect is likely due to SQSKG's ability to activate autophagy, helping to remove dysfunctional mitochondria and ROS.

Overall, it appears that the primary mechanism of SQSKG in treating CKD is its anti-fibrotic effect through autophagy activation. To further validate its anti-fibrotic effects on CKD, we used an adenine-induced CKD rat model, which allows for gradual and progressive development of renal damage.[22] This gradual onset better mimics the chronic nature of human kidney diseases by promoting crystal formation, leading to inflammation and fibrosis.[24] Our previous study demonstrated that TCM helps alleviate adenine-induced CKD progression.[12] In the current study, SQSKG showed an anti-fibrotic effect on the CKD model by reducing fibrotic factors, glomerulosclerosis, and interstitial fibrosis. Notably, this anti-fibrosis property may be linked to its effect on autophagy activation. Based on network analysis and the experiments above, we concluded that SQSKG exerts an anti-fibrotic effect by activating autophagy via suppression of the PI3K/AKT/mTOR pathway (Figure 11).

However, although network pharmacology is a potent method for comprehending the intricacies of biological systems and drug mechanisms, there are still disadvantages and challenges.[45] On the one hand, the quality of data and the

https://doi.org/10.2147/DDDT.S513824

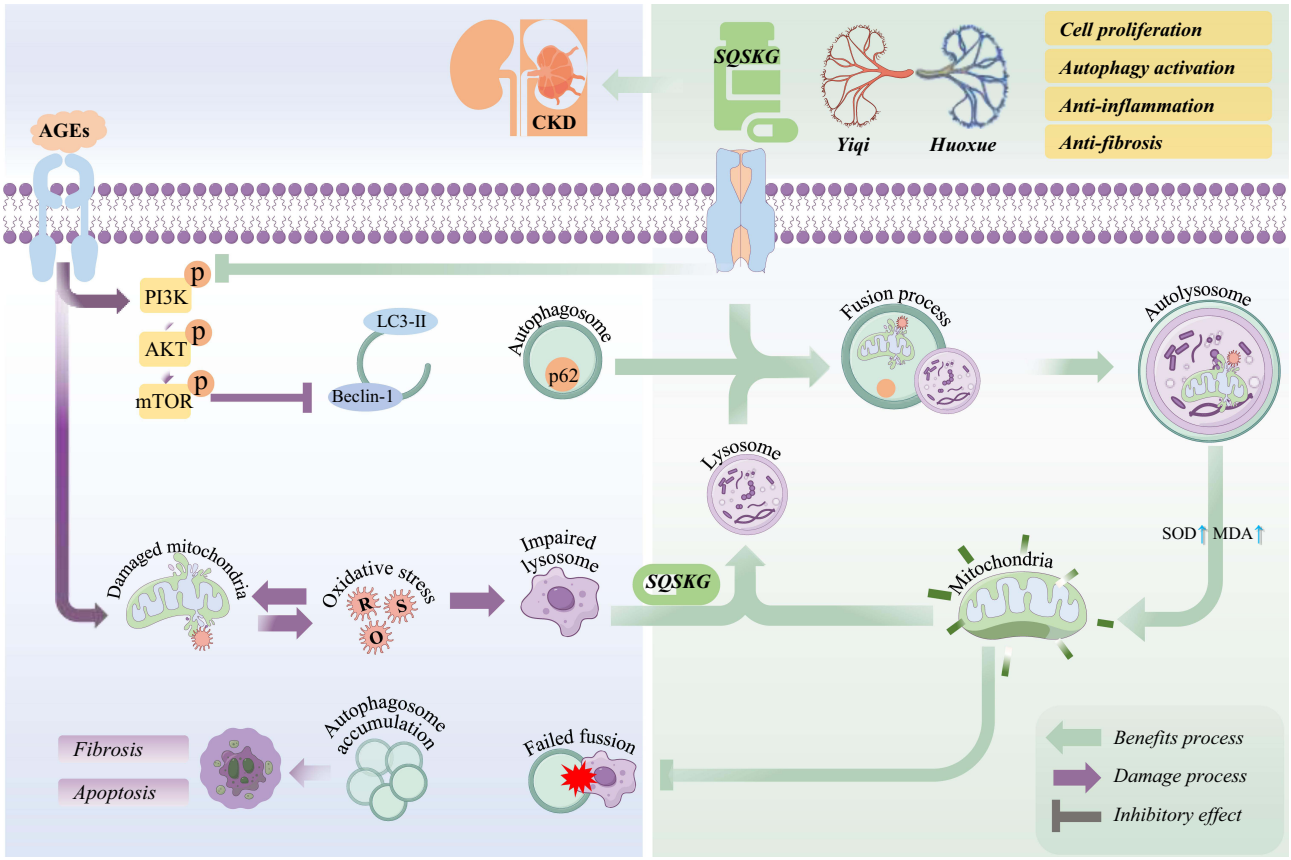

Figure 11 Potential mechanisms of the renal protective effect of Shenqi Shenkang granule (SQSKG) on chronic kidney disease (CKD). SQSKG benefits renal tubular epithelial cells exposed to risk factors by promoting autophagic induction and improving the fusion process of autophagosome and lysosome.

dynamic nature of interactions between molecules make network construction challenging and potentially inaccurate. On the other hand, the screened-out compounds cannot fully represent SQSKG. Yet, since network pharmacology remains a valuable tool for hypothesis generation and systems-level understanding of biological processes, we performed strict screening criteria during the analysis to provide a more reliable result of interaction between SQSKG and CKD. Furthermore, Vanquish UHPLC™ was applied to validate the compounds and to control quality. Moreover, the KEGG analysis indicated the involvement of AGEs-RAGE signaling in the interaction. Therefore, we employed AGEs as stimuli on HK-2 cells, aiming for a more precise correlation. After all, this study has room for improvement. Future research should incorporate pathway-specific inhibitors or genetic knockdowns to enhance mechanistic validation and reduce reliance on computational predictions. Moreover, studies are needed to optimize dosage, assess long-term safety, and explore potential synergies with existing CKD treatments to maximize the translational potential of SQSKG. Additionally, the primary compounds and other signaling pathways are worth further investigation.

Furthermore, while SQSKG shows promise for the treatment of CKD, its clinical applicability requires further investigation. Firstly, traditional use and pharmacopeia records provide a basis for dosage considerations, but adjustments are necessary according to individual factors such as age and symptom severity. Therefore, future studies should establish standardized administration guidelines and refine the optimal therapeutic window for personalized treatment. In terms of long-term efficacy, while clinical observations suggest that SQSKG improves renal function indices, long-term studies are needed to determine its efficacy in delaying the progression of CKD to ESRD in the human population. More importantly, safety remains a key concern. Although previous clinical trials have reported no significant adverse effects or changes in routine blood tests, liver function, or electrolytes following SQSKG treatment,[9] long-term clinical trials are essential to fully assess potential toxicity and ensure sustained safety. In addition, given the benefits of combining herbal

therapies with conventional treatments,[46] further research should explore the potential synergistic effects of SQSKG with standard therapy, such as RAS inhibitors and SGLT2 inhibitors.

Conclusion

This study demonstrates that SQSKG mitigates renal fibrosis by inhibiting the PI3K/AKT/mTOR pathway and promoting autophagy to restore mitochondrial homeostasis and decrease oxidative stress. These findings indicate that SQSKG could serve as an effective complementary or alternative treatment for chronic kidney disease. This research provides a novel outlook on applying the traditional Chinese medicine formula SQSKG in managing CKD.

Abbreviations

AGEs, advanced glycation end products; MDA, malondialdehyde; AKT, serine/threonine kinase 1; mTOR, mechanistic target of rapamycin; ANG, angiotensin; PAS, Periodic acid-Schiff; Bax, Bcl-2-associated X protein; PI3K, phosphoinositide 3-kinase; BSA, bovine serum albumin; PTH, parathyroid hormone; BUN, blood urea nitrogen; ROS, reactive oxygen species; caspase-3, Cysteine-aspartic acid protease-3; RTEC, renal tubular epithelial cells; CKD, Chronic kidney disease; SCR, serum creatine; Col-I, collagen-I; SOD, superoxide dismutase; DCFH-DA, 2',7'-Dichlorodihydrofluorescein diacetate; SQSKG, Shenqi Shenkang granule; DMEM, Dulbecco's modified eagle medium; TCM, traditional Chinese medicine; ESRD, end-stage renal disease; TGF-β, transforming growth factor-β; FBS, fetal bovine serum; UA, uric acid; H&E, Hematoxylin-eosin; YQHX, Yiqi Huoxue; LC3, microtubule-associated protein I light chain 3; α-SMA, α-smooth muscle actin; Masson, Masson's trichrome; β2-MG, β2-microglobulin.

Ethics Statement

The animal study was approved by the Experimental Animal Ethics Committee of Beijing University of Chinese Medicine and adhered to the ARRIVE guidelines (Permit Number: BUCM-2023090709-3229).

Author Contributions

All authors made a significant contribution to the work reported, whether that is in the conception, study design, execution, acquisition of data, analysis and interpretation, or in all these areas; took part in drafting, revising or critically reviewing the article; gave final approval of the version to be published; have agreed on the journal to which the article has been submitted; and agree to be accountable for all aspects of the work.

Funding

This work was supported by the Project of Excellent Physicians Cultivation of Beijing University of Chinese Medicine (No. Y2023B08).

Disclosure

The author(s) report no conflicts of interest in this work.

References

1. Cheng HT, Xu X, Lim PS, Hung KY. Worldwide epidemiology of diabetes-related end-stage renal disease, 2000-2015. *Diabetes Care*. 2021;44(1):89–97. doi:10.2337/dc20-1913
2. Mezzano SA, Ruiz-Ortega M, Egido J. Angiotensin II and renal fibrosis. *Hypertension*. 2001;38(3 Pt 2):635–638. doi:10.1161/hy09t1.094234
3. Panizo S, Martinez-Arias L, Alonso-Montes C, et al. Fibrosis in chronic kidney disease: pathogenesis and consequences. *Int J Mol Sci*. 2021;22(1):408. doi:10.3390/ijms22010408
4. Sang XY, Xiao JJ, Liu Q, et al. Regulators of calcineurin 1 deficiency attenuates tubulointerstitial fibrosis through improving mitochondrial fitness. *FASEB J*. 2020;34(11). doi:10.1096/fj.202000781RRR
5. Navaneethan SD, Zoungas S, Caramori ML, et al. Diabetes management in chronic kidney disease: synopsis of the KDIGO 2022 clinical practice guideline update. *Ann Intern Med*. 2023;176(3):381–387. doi:10.7326/M22-2904
6. Zhong Y, Deng Y, Chen Y, Chuang PY, Cijiang He J. Therapeutic use of traditional Chinese herbal medications for chronic kidney diseases. *Kidney Int*. 2013;84(6):1108–1118. doi:10.1038/ki.2013.276
7. Wang MR, Yu LH, Wang TT, Wang YM, Han MX. Effect of Shenqi Dihuang decoction on inflammatory factor, renal function and microcirculation in patients with early diabetic nephropathy. *Zhongguo Zhong Yao Za Zhi*. 2018;43(6):1276–1281. doi:10.19540/j.cnki.cjcmm.2018.0050

8. Wang ZB, Zou XL, Zou YX, Wang LH, Wu YT. Shenqi Dihuang Decoction inhibits high-glucose induced ferroptosis of renal tubular epithelial cells via Nrf2/HO-1/GPX4 pathway. *Zhongguo Zhong Yao Za Zhi*. 2023;48(19):5337–5344. doi:10.19540/j.cnki.cjcmm.20230721.501
9. Tan Q, Chen G, Chen S, Zeng H, Liu X, Zhu L. Effect of ShenKang granular on the expressions of serum and urine TGF-β1, miR-21 and renal function in patients with chronic kidney disease (in Chinese). *Chin J Integr Med*. 2018;19(5):391–394. doi:10.3969/j.issn.1009-587X.2018.05.006
10. Huang W, Rao Y, Li L, Li C, An Y. Clinical effect of rhubarb on the treatment of chronic renal failure: a meta-analysis. *Front Pharmacol*. 2023;14:1108861. doi:10.3389/fphar.2023.1108861
11. Zhang W, Li J, Yang P, et al. Efficacy and safety of salvia miltiorrhiza for treating chronic kidney diseases: a systematic review and meta-analysis. *Evid Based Complement Alternat Med*. 2022;2022:2117433. doi:10.1155/2022/2117433
12. Xia CH, Han XT, Zhang X, et al. Yiqihuoxue formula activates autophagy and offers renoprotection in a rat model of adenine-induced kidney disease. *Evid Based Complement Alternat Med*. 2019;2019:3423981. doi:10.1155/2019/3423981
13. Liu T, Lu X, Gao W, et al. Cardioprotection effect of Yiqi-Huoxue-Jiangzhuo formula in a chronic kidney disease mouse model associated with gut microbiota modulation and NLRP3 inflammasome inhibition. *Biomed Pharmacother*. 2022;152:113159. doi:10.1016/j.biopha.2022.113159
14. Ratliff BB, Abdulmahdi W, Pawar R, Wolin MS. Oxidant mechanisms in renal injury and disease. *Antioxid Redox Signal*. 2016;25(3):119–146. doi:10.1089/ars.2016.6665
15. Yao L, Liang X, Qiao Y, Chen B, Wang P, Liu Z. Mitochondrial dysfunction in diabetic tubulopathy. *Metabolism*. 2022;131:155195. doi:10.1016/j.metabol.2022.155195
16. Wang X, Wang ZY, Zheng JH, Li S. TCM network pharmacology: a new trend towards combining computational, experimental and clinical approaches. *Chin J Nat Med*. 2021;19(1):1–11. doi:10.1016/S1875-5364(21)60001-8
17. Wu JZ, Li YJ, Huang GR, et al. Mechanisms exploration of angelicae sinensis radix and ligusticum chuanxiong rhizoma herb-pair for liver fibrosis prevention based on network pharmacology and experimental pharmacologylogy. *Chin J Nat Med*. 2021;19(4):241–254. doi:10.1016/S1875-5364(21)60026-2
18. Piao CL, Luo JL, Jin D, et al. Utilizing network pharmacology to explore the underlying mechanism of radix salviae in diabetic retinopathy. *Chin Med*. 2019;14:58. doi:10.1186/s13020-019-0280-7
19. Jiashuo WU, Fangqing Z, Zhuangzhuang LI, Weiyi J, Yue S. Integration strategy of network pharmacology in Traditional Chinese Medicine: a narrative review. *J Tradit Chin Med*. 2022;42(3):479–486. doi:10.19852/j.cnki.jtcm.20220408.003
20. Wang Y, Wang X, Li Y, et al. Xuanfei Baidu Decoction reduces acute lung injury by regulating infiltration of neutrophils and macrophages via PD-1/IL17A pathway. *Pharmacol Res*. 2022;176:106083. doi:10.1016/j.phrs.2022.106083
21. Liu Y, Zhao P, Cai Z, et al. Buqi-Huoxue-Tongnao decoction drives gut microbiota-derived indole lactic acid to attenuate ischemic stroke via the gut-brain axis. *Chin Med*. 2024;19(1):126. doi:10.1186/s13020-024-00991-1
22. Diwan V, Brown L, Gobe GC. Adenine-induced chronic kidney disease in rats. *Nephrology*. 2018;23(1):5–11. doi:10.1111/nep.13180
23. Sengupta P. The laboratory rat: relating its age with human's. *Int J Prev Med*. 2013;4(6):624–630.
24. Diwan V, Mistry A, Gobe G, Brown L. Adenine-induced chronic kidney and cardiovascular damage in rats. *J Pharmacol Toxicol Methods*. 2013;68(2):197–207. doi:10.1016/j.vascn.2013.05.006
25. Zhang X, Hartmann P. How to calculate sample size in animal and human studies. *Front Med*. 2023;10:1215927. doi:10.3389/fmed.2023.1215927
26. Twarda-Clapa A, Olczak A, Bialkowska AM, Koziolkiewicz M. Advanced glycation end-products (AGEs): formation, chemistry, classification, receptors, and diseases related to AGEs. *Cells*. 2022;11(8):1312. doi:10.3390/cells11081312
27. Hou X, Hu Z, Xu H, et al. Advanced glycation endproducts trigger autophagy in cadiomyocyte via RAGE/PI3K/AKT/mTOR pathway. *Cardiovasc Diabetol*. 2014;13(1):78. doi:10.1186/1475-2840-13-78
28. Huang J, Chen L, Wu J, et al. Targeting the PI3K/AKT/mTOR signaling pathway in the treatment of human diseases: current status, trends, and solutions. *J Med Chem*. 2022;65(24):16033–16061. doi:10.1021/acs.jmedchem.2c01070
29. Yu JS, Cui W. Proliferation, survival and metabolism: the role of PI3K/AKT/mTOR signalling in pluripotency and cell fate determination. *Development*. 2016;143(17):3050–3060. doi:10.1242/dev.137075
30. Chen L, Li X, Deng Y, et al. The PI3K-Akt-mTOR pathway mediates renal pericyte-myofibroblast transition by enhancing glycolysis through HKII. *J Transl Med*. 2023;21(1):323. doi:10.1186/s12967-023-04167-7
31. Liu WJ, Shen TT, Chen RH, et al. Autophagy-lysosome pathway in renal tubular epithelial cells is disrupted by advanced glycation end products in diabetic nephropathy. *J Biol Chem*. 2015;290(33):20499–20510. doi:10.1074/jbc.M115.666354
32. Jia M, Qiu H, Lin L, Zhang S, Li D, Jin D. Inhibition of PI3K/AKT/mTOR signalling pathway activates autophagy and suppresses peritoneal fibrosis in the process of peritoneal dialysis. *Front Physiol*. 2022;13:778479. doi:10.3389/fphys.2022.778479
33. Dong R, Zhang X, Liu Y, et al. Rutin alleviates EndMT by restoring autophagy through inhibiting HDAC1 via PI3K/AKT/mTOR pathway in diabetic kidney disease. *Phytomedicine*. 2023;112:154700. doi:10.1016/j.phymed.2023.154700
34. Kimura T, Isaka Y, Yoshimori T. Autophagy and kidney inflammation. *Autophagy*. 2017;13(6):997–1003. doi:10.1080/15548627.2017.1309485
35. Tang C, Livingston MJ, Liu Z, Dong Z. Autophagy in kidney homeostasis and disease. *Nat Rev Nephrol*. 2020;16(9):489–508. doi:10.1038/s41581-020-0309-2
36. Chang M, Shi X, Ma S, et al. Inhibition of excessive autophagy alleviates renal injury and inflammation in a rat model of immunoglobulin A nephropathy. *Eur J Pharmacol*. 2023;961:176198. doi:10.1016/j.ejphar.2023.176198
37. Kang R, Zeh HJ, Lotze MT, Tang D. The Beclin 1 network regulates autophagy and apoptosis. *Cell Death Differ*. 2011;18(4):571–580. doi:10.1038/cdd.2010.191
38. Kim YC, Guan KL. mTOR: a pharmacologic target for autophagy regulation. *J Clin Invest*. 2015;125(1):25–32. doi:10.1172/JCI73939
39. Tan AL, Forbes JM, Cooper ME. AGE, RAGE, and ROS in diabetic nephropathy. *Semin Nephrol*. 2007;27(2):130–143. doi:10.1016/j.semnephrol.2007.01.006
40. Ward MS, Fortheringham AK, Cooper ME, Forbes JM. Targeting advanced glycation endproducts and mitochondrial dysfunction in cardiovascular disease. *Curr Opin Pharmacol*. 2013;13(4):654–661. doi:10.1016/j.coph.2013.06.009
41. Hara H, Araya J, Ito S, et al. Mitochondrial fragmentation in cigarette smoke-induced bronchial epithelial cell senescence. *Am J Physiol Lung Cell Mol Physiol*. 2013;305(10):L737–46. doi:10.1152/ajplung.00146.2013
42. Bhatti JS, Bhatti GK, Reddy PH. Mitochondrial dysfunction and oxidative stress in metabolic disorders - A step towards mitochondria based therapeutic strategies. *Biochim Biophys Acta Mol Basis Dis*. 2017;1863(5):1066–1077. doi:10.1016/j.bbadis.2016.11.010

43. van der Bliek AM, Shen Q, Kawajiri S. Mechanisms of mitochondrial fission and fusion. *Cold Spring Harb Perspect Biol*. 2013;5(6):a011072–a011072. doi:10.1101/cshperspect.a011072
44. Chen W, Zhao H, Li Y. Mitochondrial dynamics in health and disease: mechanisms and potential targets. *Signal Transduct Target Ther*. 2023;8(1):333. doi:10.1038/s41392-023-01547-9
45. Zhao L, Zhang H, Li N, et al. Network pharmacology, a promising approach to reveal the pharmacology mechanism of Chinese medicine formula. *J Ethnopharmacol*. 2023;309:116306. doi:10.1016/j.jep.2023.116306
46. Patankar S, Gorde A, Patankar S, et al. A prospective, randomized, open label, parallel group, comparative clinical trial to evaluate the safety and efficacy of combination of herbal oral capsule and rectal medication to improve gut health of type 2 diabetic patients having chronic kidney disease (CKD). *J Ayurveda Integr Med*. 2025;16(2):100992. doi:10.1016/j.jaim.2024.100992